AD 294 920

63-2-3

294 920

AIR FORCE INSTITUTE OF TECHNOLOGY

AIR UNIVERSITY
UNITED STATES AIR FORCE

SCHOOL OF ENGINEERING

WRIGHT–PATTERSON AIR FORCE BASE, OHIO

AF-WP-O-MAY 62 3,500

THESIS

Presented to the Faculty of the School of Engineering of

the Air Force Institute of Technology

Air University

in Partial Fulfillment of the

Requirements for the Degree of

Master of Science

AN EVALUATION OF FOUR METHODS FOR CONVERTING SINGLE AXIS PILOT RATINGS TO MULTI-AXIS PILOT RATINGS USING FIXED BASE SIMULATION DATA

Vernon Allan Dander Captain, USAF
GE/EE/62-4

Graduate Electronics

December 1962

Preface

This study was conducted at the suggestion of Mr. R. J. Wasicko of the Flight Control Laboratory, Aeronautical Systems Division. As head of the Handling Qualities Section, he was very interested in developing methods to utilize the expensive experimental data that had been accumulated in previous studies. My interest in improving handling qualities, after flying helicopters for more than a thousand hours, was a more personal one.

I wish to express my appreciation to those on the staff of the Flight Control Laboratory who aided my efforts; to Mr. Wasicko, my thesis sponsor, for his suggestions and guidance; to Mr. P. E. Pietrzak for his aid in the experimental work; and to Messrs. R. R. Davis and Virgil Faught who supplied most of the facilities and equipment. My thanks are due also to my Faculty Thesis Advisor, Prof. J. J. D'Azzo, for his guidance and advice.

My special thanks go to Mr. Fred Thomas of the Flight Control Laboratory, who served as the test subject. His cooperation and efforts to keep the time span for taking the experimental data as short as possible is especially appreciated.

Vernon A. Dander

Contents

Contents

List of Figures

List of Figures

List of Tables

Abstract

This study evaluated four possible techniques for combining single axis pilot ratings to predict a pilot rating for the axes in combination. Two of the methods proved promising, giving good results for the experimental data taken during the study. The first, developed by I. L. Ashkenas, is based on a non-linear relationship between the pilot rating and the pilot lead time-constant. The second, based on the incremental change of pilot rating as the vehicle handling qualities are changed, gives comparable results, but is restricted as to the data to which it can be applied. An attempt to improve the results of the two methods by combining certain features of each proved to be unfruitful. The fourth method, based on the summation of the individual axes ratings, was shown to be useless.

AN EVALUATION OF FOUR METHODS FOR CONVERTING SINGLE AXIS PILOT RATINGS TO MULTI-AXIS PILOT RATINGS USING FIXED-BASE SIMULATION DATA

I. Introduction

Because the term "handling qualities" has a vague rather than concrete meaning, assessment of these qualities is subjective rather than objective or quantitative. However, experience has shown that such assessments are dependent on definable vehicle stability and control characteristics. To the pilot, the three characteristics that are of primary importance are the closed loop response, the open loop characteristics, and the maneuvering capabilities of the system.

Of particular interest is the closed loop response because the pilot is an active participant in the control system, acting as a vocal, adaptive controller. Since he is aware of his role and performance in the system, his opinion (quantized as a "pilot rating") of its handling qualities is a dominant consideration in assessing the overall pilot-vehicle performance.

A pilot-vehicle system theory of handling qualities has been developed and extensive analysis (Ref 3, 5) has been made for single axis situations. The method has progressed to the point of being able to predict pilot

ratings for single axis tasks. During the development and verification of the theory, a considerable amount of single axis experimental data has been accumulated.

However, actual flight situations require simultaneous control of more than one axis. In extending the single axis theory to multiple axis tasks, it would be desirable to utilize the information gathered in the single axis experiments rather than to simulate a large number of multi-axis configurations. The question arises, however, as to how to combine the single axis data to determine a rating for a multi-axis task.

The object of this thesis was to evaluate various techniques that might be used. The approach was to gather single and related multi-axis data and then compare the multi-axis ratings predicted by each method with the actual multi-axis ratings.

The pilot's rating of the handling qualities of a vehicle is influenced by the dynamic characteristics of the vehicle. In conventional aircraft, helicopters, and spacecraft, both electronic and mechanical stability augmentation systems are used to improve the dynamic characteristics when the aerodynamic response characteristics are poor. Thus, it is possible to classify changes in the handling qualities of a "simulated" vehicle as relative changes in the degree or amount of

augmentation. In this study a low level of augmentation implies the poorest handling qualities being considered, while a high level implies the best handling qualities evaluated.

Scope of Study

This thesis evaluated four possible techniques for converting pilot rating (PR) data for separate single axes into pilot ratings for the axes in combination. The study was limited to an uncoupled, three axis, fixed base simulation. The vehicle transfer characteristics were derived from the linearized equations of motion of a tandem rotor helicopter in "up and away", straight and level flight. The only criterion for the "goodness" of a particular configuration was the pilot rating.

Plan of Development

The pilot model transfer function and adaptation techniques for a compensatory-tracking task are reviewed briefly. A modified form of the Cooper scale is presented and comments made as to why it was used. The four methods to be evaluated are explained in detail with illustrative examples. The experimental set-up, run procedures and sequence, and operator training are discussed. The methods used to analyse the data are explained. Comparisons of the four methods and recommendations for further study are made.

II. Pilot Representation and Cooper Scale

The generally accepted servo representation of a closed loop control system with the pilot performing a compensatory-tracking task is shown in Figure 1.

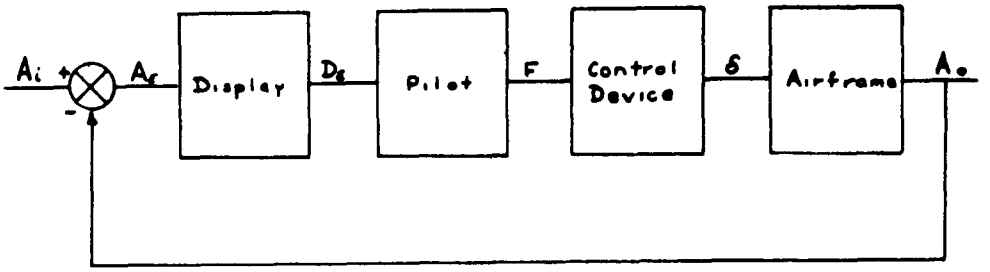

Figure 1

Compensatory-tracking, Closed Loop Block Diagram

In a compensatory-tracking task the pilot observes only the displayed error D_ϵ, which is the difference between the input A_i and the airframe output A_o. The pilot's output is a force F which produces a control surface deflection δ through the control device. The pilot transfer function G_p is usually defined as

$$G_p(S) = \frac{F(S)}{D(S)} = \frac{K_p e^{-\tau S}(T_L S + 1)}{(T_I S + 1)(T_N S + 1)}$$

where

K_P = Pilot gain

τ = Pilot reaction time delay

T_L = Pilot lead time-constant

T_I = Pilot lag time-constant

T_N = First-order time-constant approximating pilot's neuro-muscular lags

When closing the loop, the pilot adopts the form of equalizing characteristics that insures stable control. Once good low frequency, closed-loop response has been achieved with the lag term, he generates whatever lead is necessary to retain high frequency system stability (Ref 3:7). The pilot lead time-constant associated with this generated lead is an important parameter used in the solutions for predicted pilot rating in two of the methods to be evaluated.

Cooper Scale

In order to have some common standard for aircraft handling qualities, G. E. Cooper proposed a pilot opinion rating scale in 1957 (Ref 4:48). This scale has become generally accepted for test flight and simulator evaluation of flying vehicles. A modified form of the Cooper scale (Table I), used by Systems Technology, Inc. in their handling qualities study of single-loop roll tracking tasks, was used in this experiment. The adjective terms

of this scale were more useful to a pilot with a relatively low level of flying experience than those of the original scale.

Table I
Modified Cooper Scale

Category	Rating	Flight Conditions
	1	EXCELLENT - pleasureable to fly
Satisfactory	2	GOOD - easy to track - no annoyances
	3	GOOD - easy to track - vaguely unpleasant characteristics
	4	ACCEPTABLE - tracks fairly well, but has some definitely unpleasant characteristics
Unsatisfactory	5	UNDESIRABLE - for normal operation - tracking can be made acceptable only with effort
	6	UNACCEPTABLE - except for emergency - tracking is difficult and requires much attention
	7	UNACCEPTABLE - even for emergency - tracking is poor and requires full attention
Unacceptable	8	DANGEROUS - incipient loss of control
	9	UNCONTROLLABLE - for more than several seconds
	10	LOST CONTROL - every time - absolutely uncontrollable

(Ref 5:62)

III. Explanation of Methods

Method #1

The simplest method of combining two or more single axis pilot ratings into a predicted pilot rating for the combined axes is to sum all the single axis ratings. The general mathematical expression for this method is

$$(PR)_M = \sum_{i=1}^{N} (PR)_i$$

where

$(PR)_M$ = Pilot rating for the multiple axis configuration

$(PR)_i$ = Pilot rating for the i^{th} single axis configuration

N = Number of single axes making up the multiple axis configuration.

It should be apparent that this method is not too promising. In the example in Table II, three single axis ratings in the "good" flight condition region sum to a predicted rating in the "unacceptable" region. It is not likely that the pilot would consider the handling qualities of the vehicle had deteriorated that much. However, the method is evaluated in this thesis for comparison with the other methods.

Table II
Example of Method #1

Axis (i)	Pilot Rating
1	$(PR)_1 = 2$
2	$(PR)_2 = 2$
3	$(PR)_3 = 2.5$
1, 2, and 3	$(PR)_M = 6.5$

Method #2

A second possible technique for predicting multi-axis ratings is to take into account only the incremental effects on the pilot's rating of a change in the augmentation in any axis or axes. The sum of these increments can be added to some measured or estimated "best" multi-axis configuration to find the predicted pilot rating. The general equation for this method is

$$(PR)_M = (PR)_{Best} + \sum_{i=1}^{N} (\Delta PR)_i$$

where

$(PR)_{Best}$ = Pilot rating for the "best" multiple axis configuration

$(\Delta PR)_i$ = Incremental pilot rating between the best i^{th} single axis configuration and the i^{th} single axis configuration making up the multiple axis configuration

In the example of Method #2 shown in Table III

H = Highest level of augmentation in any axis

M = Medium level of augmentation in any axis

N = 3

Table III
Example of Method #2

	Augmentation			$(\Delta PR)_i$			$(PR)_{Best}$	Predicted PR
Axis / Configuration	-	2	3	1	2	3	Combined Axes	Combined - Axes
A	H	H	H				3	
B	H	H	M			1	3	4
C	H	M	M		2	1	3	6

In configuration A the $(PR)_{Best}$ is established from the measured pilot rating, in this example 3, for the three axes in combination with the augmentation of each axis set at the "H" level. In configuration B the measured change of rating when going from the "H" to "M" level in axis 3 is 1 rating point. This increment - $(\Delta PR)_3$- is added to the $(PR)_{Best}$ rating giving a predicted rating of 4. In configuration C the augmentation of axis 2 has also been changed from "H" to "M", but with a measured change of rating of 2 in this case. The predicted rating is 6 or the sum of the $(PR)_{Best}$ rating of 3 plus the $(\Delta PR)_3$ of 1 and the $(\Delta PR)_2$ of 2.

Method #3

A third possibility is that a predicted rating can be found through a non-linear variation of pilot rating with another measurable parameter. Such a method has been proposed by I. L. Ashkenas (Ref 11:10). From his studies of longitudinal handling qualities (Ref 9:26-31) he has found that there seems to be a non-linear relationship where the change of pilot rating is a function of the pilot generated lead time constant T_L. The graphical representation of the function is a band curve approximately two rating points wide (Figure 3), taken from reference 11. In this thesis the center-line of the curve was used for calculations.

The general equation for this method is

$$(PR)_m = f\left[(T_L)_{Base} + \left\{ f^{-1}[(PR)_i] - (T_L)_{Base} \right\} \right]$$

where

$$PR = f\left[T_L\right] \qquad \text{and} \qquad T_L = f^{-1}\left[PR\right]$$

define the non-linear relationship between PR and T_L shown in Figure 3 and

$$(T_L)_{Base} = f^{-1}\left[\text{Best single axis PR}\right]$$

A graphical solution for method #3 is shown in Figures 2 and 3. Because axis (2) has a higher pilot rating than the other axis at the highest augmentation level (H), a PR base-line, shown by a dashed line, is

(Adapted from Ref 11)

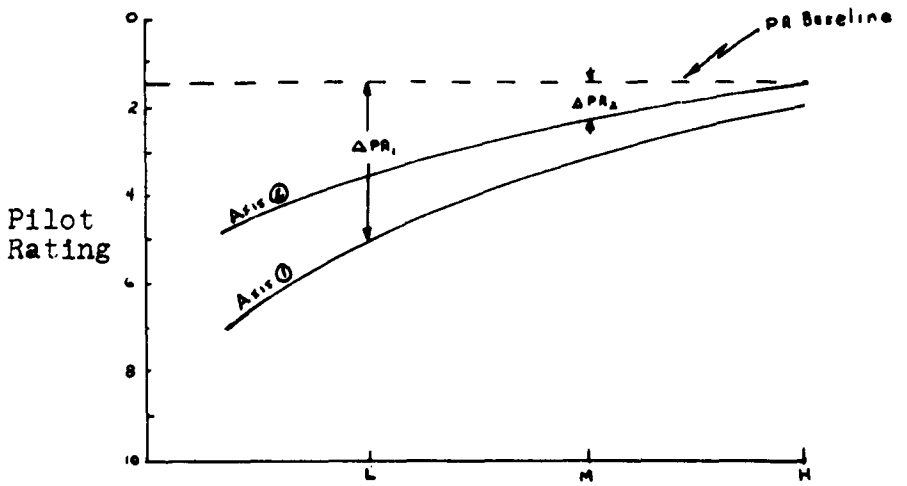

Level of Damping Augmentation

Figure 2

Variation of Pilot Rating with Damping Level

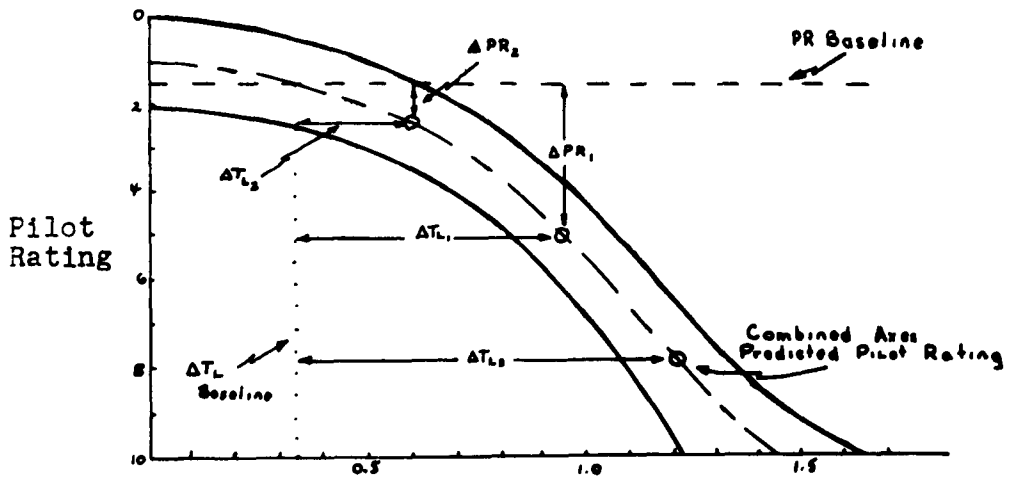

Pilot Lead Time-constant, T_L

Figure 3

"Ashkenas Curve"
Variation of Pilot Rating with Pilot Lead Time-constant

established at this rating and is transferred to Figure 3 at the same value of pilot rating. The intersection of the PR base-line and the center-line of the conversion curve determines the base-line for increments of pilot lead time-constant (dotted line). The predicted pilot rating is then determined as follows:

1. Find, at the level of augmentation of each axis in Figure 2, the PR difference (ΔPR) between the individual axes (1) and (2) and the PR base-line. In this illustration axis (1) is measured at the lowest level (L) and axis (2) is measured at the medium level (M).
2. Lay off the values of ΔPR from the PR base-line to the center-line of the conversion curve of Figure 3 and determine the corresponding pilot lead time increments (ΔT_{L1} and ΔT_{L2}) from the pilot lead time base-line.
3. Add the increments of pilot lead time and lay off this value (ΔT_{L3}) from the pilot lead time base-line to the conversion curve. The pilot rating at the point of intersection is the predicted pilot rating for the combined axes.

Method #4

A fourth method is to combine the techniques of methods #2 and #3. The incremental changes of pilot lead time-constant are determined from the changes of pilot rating in each axis as a result of the augmentation changes. The predicted pilot rating is then determined by adding the appropriate increments to a pilot lead time-constant base-line that is determined from a measured or estimated "best" combined axis pilot rating. The general equation for method #4 is

$$(PR)_M = f\left[(T_L)_{Best} + \left\{ f^{-1}[(PR)_i] - (T_L)_{Base} \right\} \right]$$

where

$$(T_L)_{Best} = f^{-1}\left[(PR)_{Best} \right]$$

Method #4 is graphically illustrated in Figures 4 and 5. In this example, the "best" pilot rating for the combined axes is 3 (a measured value in this thesis) and the PR differences are both measured at the medium augmentation level. To determine predicted pilot rating:

1. Follow the procedures for method #3 through step 2.
2. Establish a combined ΔT_L base-line based on the "best" combined axis rating by drawing a vertical line on Figure 5 (alternate dots and dashes) from the intersection of the "best" combined axis

pilot rating line (alternate dots and double dashes) with the center-line of the conversion curve.

3. Add the increments of pilot lead time and lay off this value (ΔT_{L3}) from the combined ΔT_L base-line to the conversion curve. The pilot rating at the point of intersection determines the predicted pilot rating of the combined axes.

(Adapted from Ref 11)

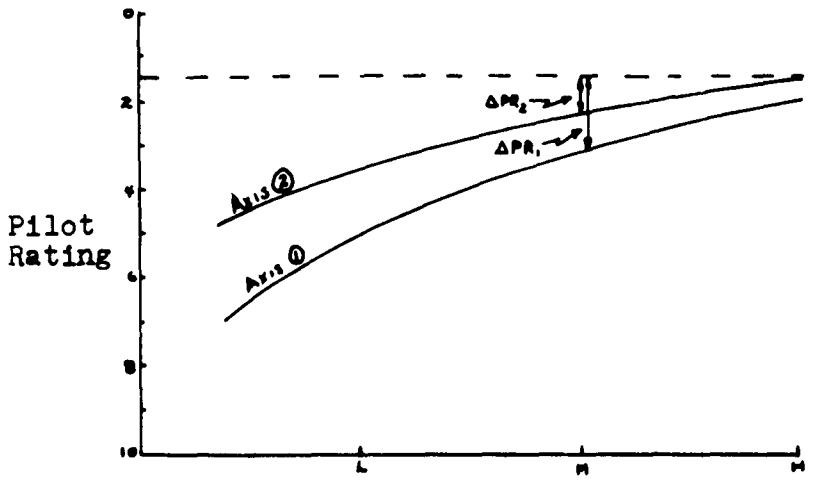

Level of Damping Augmentation

Figure 4

Variation of Pilot Rating with Damping Level

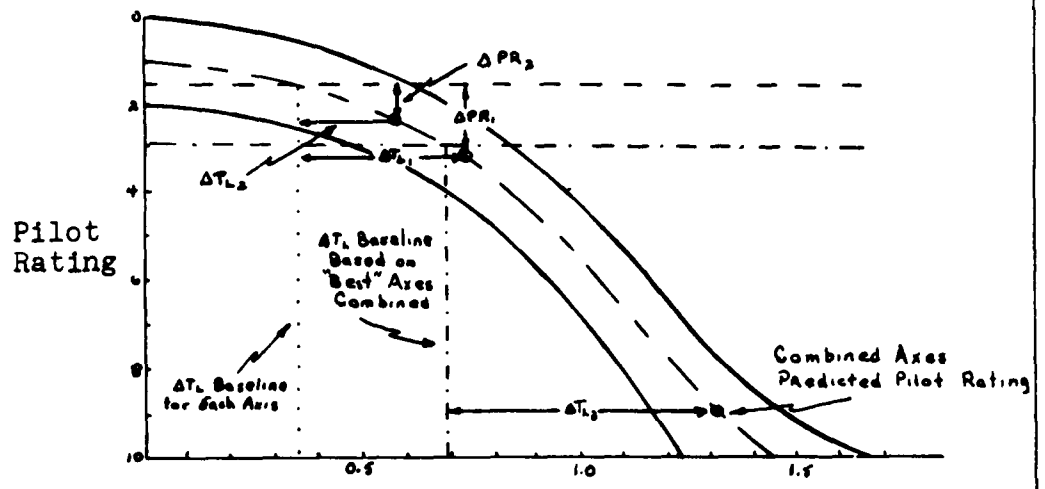

Pilot Lead Time-constant, T_L

Figure 5

"Ashkenas Curve"
Variation of Pilot Rating with Pilot Lead Time-constant

IV. Experimental Procedure

Equipment Set-up

A servo model of the closed loop, compensatory-tracking control system used in this experiment is shown in block diagram form in Figure 6. The three uncoupled loops represent pitch, Θ , bank, ϕ , and sideslip, φ . Sideslip was used instead of yaw in an attempt to relate the dynamics more closely to an output that would be a function of just rudder control. The block labeled G_p represents the pilot transfer function, while G_Θ, G_ϕ, and G_φ represent the transfer characteristics of the controlled element in each loop.

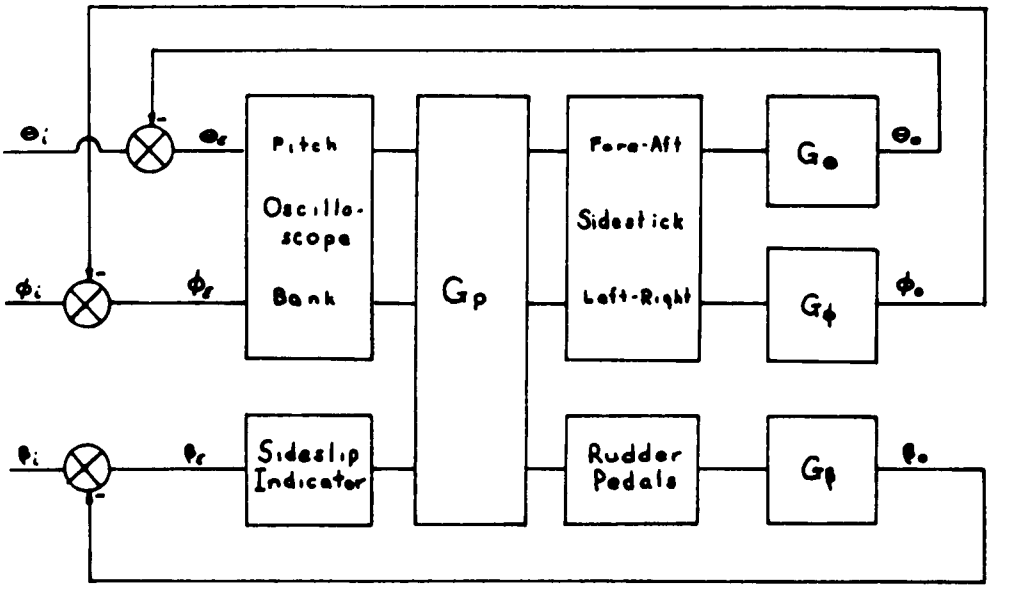

Figure 6

Servo Model with Three Uncoupled Loops

The inputs into the system (Θ_i , Φ_i , β_i) were generated by random signals which were compared with the outputs of the respective feedback loops. An error signal (Θ_ϵ , Φ_ϵ , β_ϵ) was fed as a voltage to the display. The display for pitch and bank error appeared as a 2 inch horizontal bar on an oscilloscope. Pitch error was indicated as a vertical displacement of the bar, up or down, from the center of the oscilloscope. Bank error was displayed as a tilting of the bar about the vertical center-line of the scope. Horizontal and vertical center-lines were scribed on an overlay on the face of the oscilloscope with intervals marked every .1 inch. Sideslip error was displayed as a needle deflection on a dial directly below the scope. The face of the dial was marked at intervals to the left and right of the vertical zero position; however, no significance was given to the numbers on the dial and each mark was considered an arbitrary unit. Because the pilot found it easier to fly, an "outside-in" display was provided on the scope. Thus, the bar was flown back to the horizontal center-line of the scope. He also found it easier to associate the deflection of the sideslip needle to one side with the rudder pedal on that side so an "inside-out" presentation was used in sideslip.

The angular deflection of the sidestick and fore-aft displacement of the rudder pedals by the pilot

produced an output voltage in each channel directly proportional to the amount of the movement. These voltages were fed to the appropriate controlled element.

The controlled elements were simulated on an analog computer. One parameter of each controlled element was changed to produce three different response characteristics in each channel. The three were considered as high (H), medium (M), and low (L) levels of augmentation in each channel. The transfer functions used for the controlled elements were

$$G_\theta(S) = \frac{\Theta(S)}{\delta_{e_s}(S)} = \frac{4(S+.04)(S+.9)}{(S+1/T_{p_\theta})(S+5)\left[S^2+2(.7)(.25)S+.25^2\right]}$$

with $1/T_{p_\theta} = 0$ for H, $1/T_{p_\theta} = -.5$ for M, and $1/T_{p_\theta} = -.8$ for L

$$G_\phi(S) = \frac{\phi(S)}{\delta_{a_s}(S)} = \frac{.5(S+.1)}{(S+1.5)\left[S^2+2\zeta_\phi(.5)S+.5^2\right]}$$

with $\zeta_\phi = +.84$ for H, $\zeta_\phi = -.3$ for M, and $\zeta_\phi = -.84$ for L

$$G_\beta(S) = \frac{\beta(S)}{\delta_{r_p}(S)} = \frac{10(S+.1)}{(S+3)\left[S^2+2\zeta_\beta(.5)S+.5^2\right]}$$

with $\zeta_\beta = +.5$ for H, $\zeta_\beta = -.2$ for M, and $\zeta_\beta = -.5$ for L

The input signals were summations of non-harmonic, low-frequency sine waves. Four waves were summed for pitch and bank and three waves summed for sideslip (Figure A-2). The amplitudes and frequencies used produced a signal sufficiently random for the experiment.

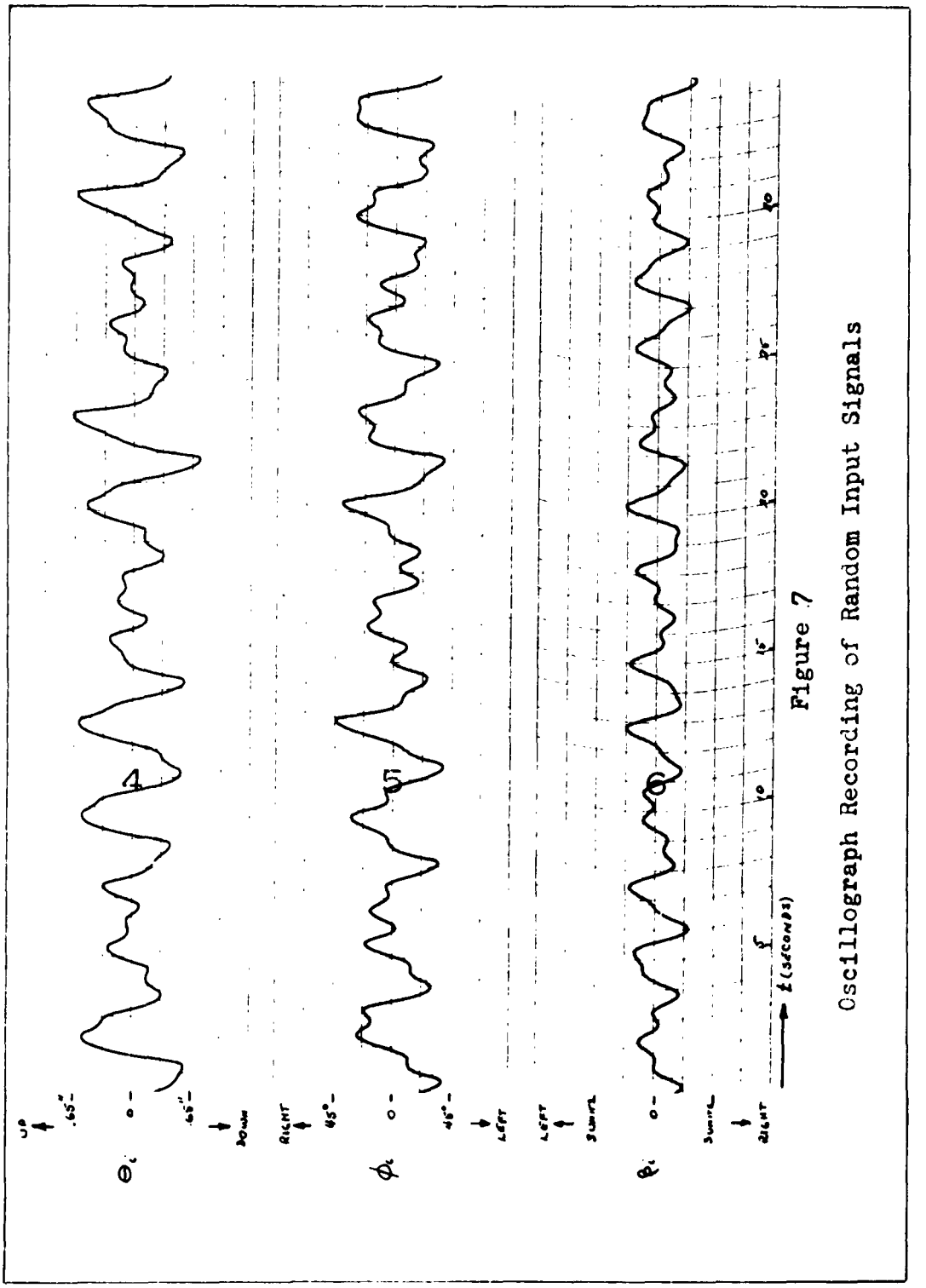

Figure 7

Oscillograph Recording of Random Input Signals

The maximum amplitudes of the signals produced approximately ±.75 inches of displayed pitch travel, ±45 degrees of displayed bank angle, and ±1.8 units of sideslip needle deflection. Figure 7 is a sample simultaneous trace of the input signals.

Run Procedures

The pilot was instructed to try and maintain the bar level at the intersection of the scope center-lines and to maintain the sideslip needle pointer at zero. After a run had been completed with a particular configuration of the augmentation levels, the pilot was asked to rate it on the basis of his interpretation of the modified Cooper scale. If he lost control of the simulator during the run, the computer was stopped prior to overload. The pilot was then given the option of repeating the same configuration again until he was satisfied he could rate it. It was felt that this would give better differentiation of the worst cases. It was also assumed that the pilot would take into account in his rating any improvement in his ability to fly the configuration due to fore-knowledge from the previous run. He was not advised during the course of the experiment about control techniques, the nature of the augmentation and how it was derived, or the consistency of his ratings. A brief warm-up period was given prior to each session

and frequent rest periods were scheduled throughout the runs.

Operator Training

Time limitations precluded the training of more than one pilot for the experiment. The pilot, an aeronautical engineer, had approximately 180 flying hours in light aircraft and about 10 simulation hours on previous studies. In the three days prior to the data runs he flew 150 training runs in the single and three axis configurations. The sequence of these runs was random and a sufficient number of repeated runs were included to determine the consistency of his ratings. The values used for the augmentation levels were not those used for the data runs.

An analysis of the first training runs showed a definite tendency to give a much better rating to a repeated configuration as the pilot became more proficient in flying the simulator. However, at the end of the third day he was consistently rating repeat runs to within an increment of ± 1. This was considered a reasonable spread and was compensated for to some extent in the data runs by averaging the ratings for any particular configuration.

Data Run Sequence

Data for the three axis analysis were taken during the two day period immediately following the training runs. Twenty-one single axis runs of 120 seconds duration, followed by fifty-three axis runs of 120 seconds duration, were flown the first day. The next day thirty-six three axis runs of 120 seconds duration were followed by twenty-four single axis runs of 60 seconds duration. All single axis runs were completed, but twenty-eight of the three axis configurations were not completed on the first attempt. The pilot exercised the re-run option thirty-six times, repeating some configurations more than once.

Because the three axis cases showed a preponderance of data at the higher end of the rating scale, a group of two axis runs with single axis checks were flown after a three day delay. Eighteen single axis runs (60 seconds) and twenty-nine two axis runs (120 seconds) were flown in one day. Unfortunately, prior to these runs, it was necessary to change a turret resistor in the pitch circuit of the computer. Although the same numerical setting was used on the replacement, there was a definite overall improvement in the pitch characteristics. The single axis runs of this session show that the relative rating position of each augmentation

level remained the same, but there was a large change in the increment of pilot rating between each level. Since the bank ratings remained essentially unchanged, it was assumed that the change in ratings was due to a change in the circuit and not a variation in the pilot. The single axis ratings taken prior to the component change indicate that the resistor was a fixed value during the three axis data runs and was not varying throughout the experiment.

Since the procedures evaluated in this study do not require particular values in any axis, the two groups of data were considered as valid separate experiments and evaluated accordingly.

V. Analysis of the Data

Statistical Methods Used in Analysis

The first step in analyzing the four methods was to calculate the predicted pilot ratings for all configurations. These were then compared with the actual pilot ratings and a scatter diagram was plotted for each method. A scatter diagram is a graphical representation of two related series with one variable scaled on the X axis and the other scaled on the Y axis. If the paired values of the two series are plotted in the XY plane, the result is a scatter diagram. In this thesis the actual pilot ratings were scaled on the X axis and the predicted pilot ratings were scaled on the Y axis.

A line of perfect correlation was then plotted on the scatter diagram. This line would be the locus of all points if there were perfect correlation or agreement between the predicted and actual pilot ratings. Since both axes have the same scale, the perfect correlation curve is a straight line represented by an equation of the form

$$Y = a + bX$$

where $a = 0$ and $b = 1$.

Next, a line of regression was calculated for the plotted data points. The line of regression is a curve, passing through the plotted points, that best describes the trend of the data. If a straight line trend is assumed, the line of trend will be represented by an equation of the same type as the line of perfect correlation. If the values of a and b are evaluated, they can be compared with the "perfect" values of the correlation line. To solve for these values, the principle of least squares is used. This principle states that "A line of best fit to a series of values is a line the sum of the squares of the deviations (the differences between the line and the actual values) about which will be a minimum" (Ref 1:52).

To solve for a and b the following values are determined:

$$\sum(Y) \; ; \; \sum(X) \; ; \; \sum(XY) \; ; \; \sum(X^2) \; ; \; N$$

where N is the number of paired values being considered. These values are substituted into the following equations which are solved simultaneously:

$$\sum(Y) = N a + b \sum(X)$$

$$\sum(XY) = a \sum(X) + b \sum(X^2)$$

The line of regression was then plotted on the scatter diagrams. Comparison of the correlation line and the regression line, which will be discussed more fully in subsequent sections, indicated that only two of the methods gave good results. It was decided to investigate these two cases further by calculating the sample variance of the data points about the line of perfect correlation. This gives a numerical value to the scatter or variation of the data points about the line of correlation, which is a figure of the relative merit of the methods in predicting the correct pilot rating. The sample variance of the data points about the line of perfect correlation was calculated from the formula

$$\sigma^2_{Correlation} = \frac{1}{N}\sum (Y - Y_{Correlation})^2$$

Analysis of Pilot Consistency

Figures 8, 9, 10, and 11 show the pilot's ability to repeat ratings for the same configurations. The points were arrived at by comparing the first rating of the configuration with the second, the second with the third, and so on. The "old" rating was scaled on the X axis and the "new" rating on the Y axis. Any tendency of the pilot to change his rating as he progressed through

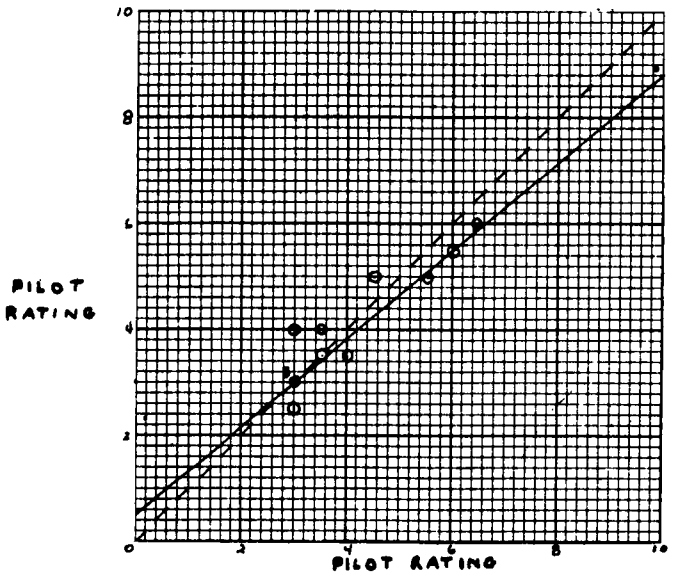

Figure 8

Single Axis Repetition for Two Axis Experiment

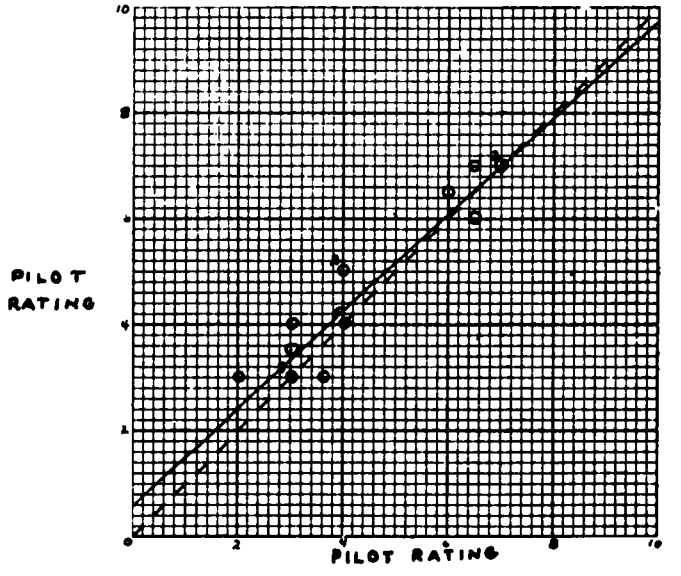

Figure 9

Two Axis Repetition

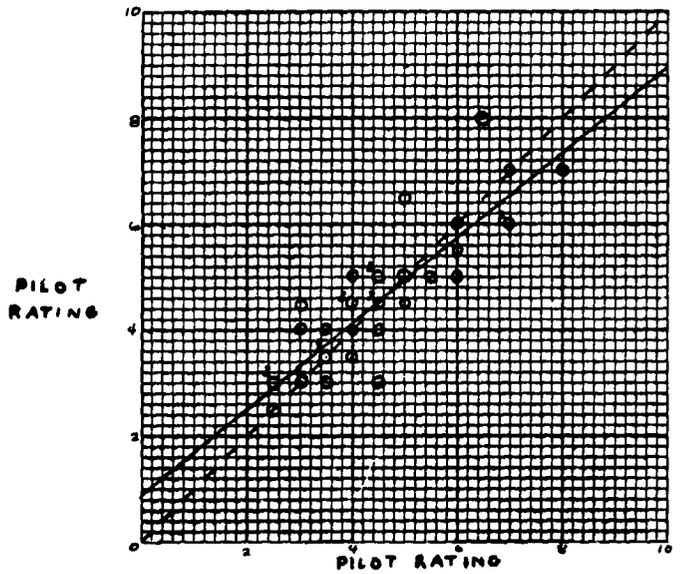

Figure 10

Single Axis Repetition for Three Axis Experiment

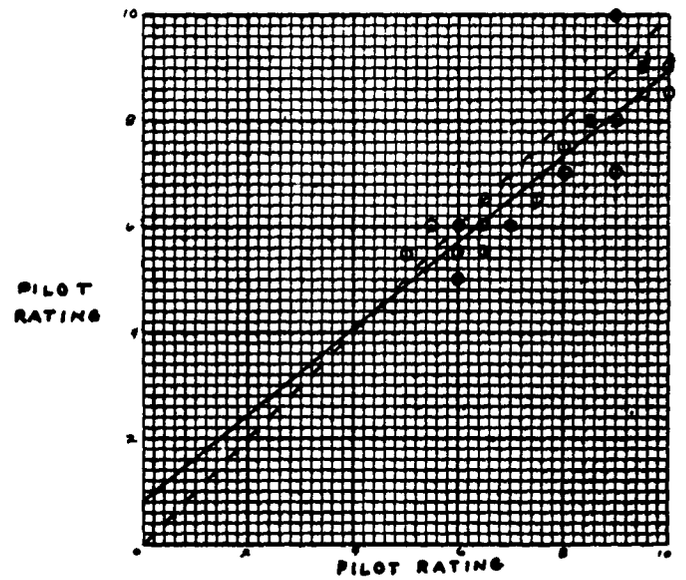

Figure 11

Three Axis Repetition

the sessions is reflected in the shift of the data points above or below the line of perfect correlation.

An examination of all four figures shows that the pilot had a tendency to rate the "poor" configurations slightly better and the "good" configurations slightly worse as he progressed through the experiments. The trend of the ratings is seen from the lines of regression which are plotted as solid lines on all the figures. The pilot was excellent in his ability to repeat ratings within ± 1 rating points. All of the cases for the two axis experiment were within this range. In the three axis experiment, 89% of the single axis repeats and 91.5% of the three axis repeats were within ± 1.

Analysis of Method #1

As anticipated, method #1 is useless for predicting pilot rating. Figures 12, 13, and 14 show that the line of regression is nowhere near the perfect correlation line and the method consistently predicts ratings that are higher than the actual ones. The values of (a) and (b) for the line of regression are given in Table IV.

Table IV
Method #1, Slope (b) and Y Intercept (a) for Line of Regression

	a	b
Two axis data	4.84	.6788
Three axis data	9.71	.0325
Combined data	6.32	.4250

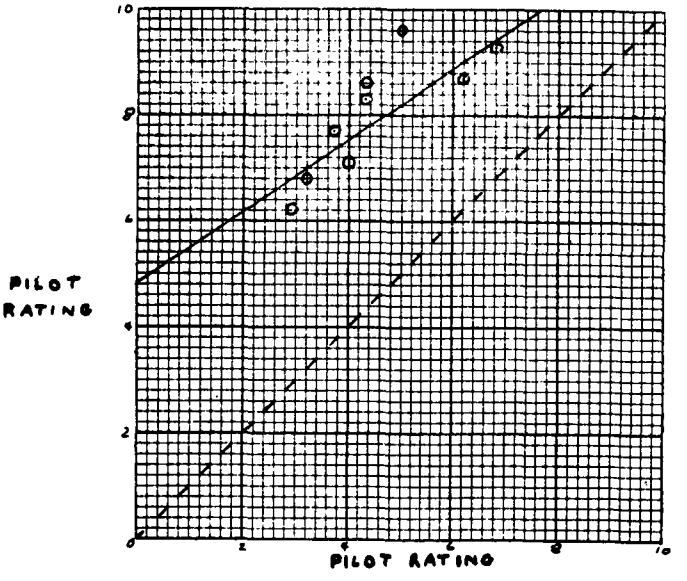

Figure 12

Method #1, Two Axis Scatter Diagram

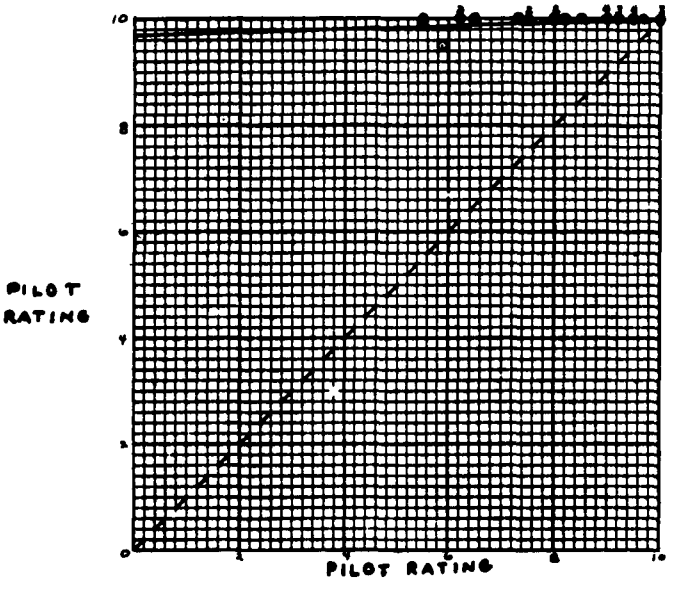

Figure 13

Method #1, Three Axis Scatter Diagram

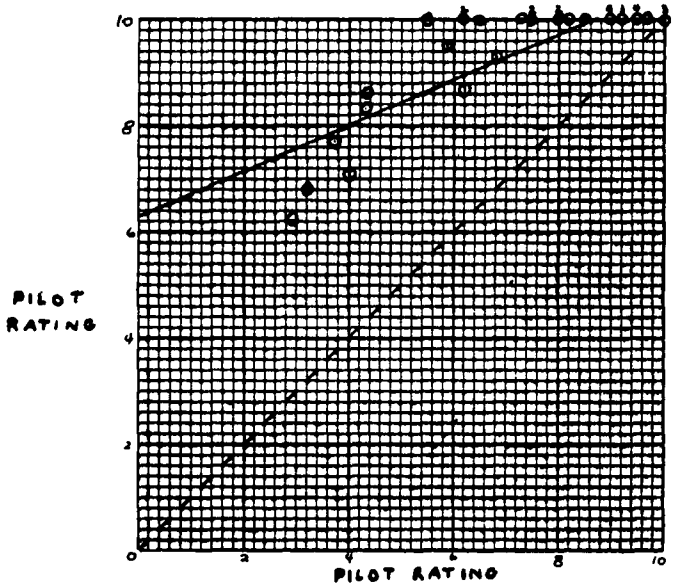

Figure 14

Method #1, Combined Data Scatter Diagram

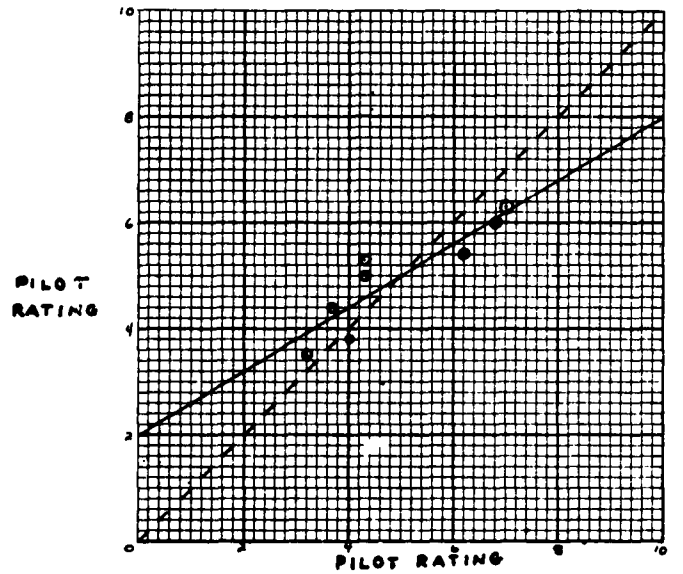

Figure 15

Method #2, Two Axis Scatter Diagram

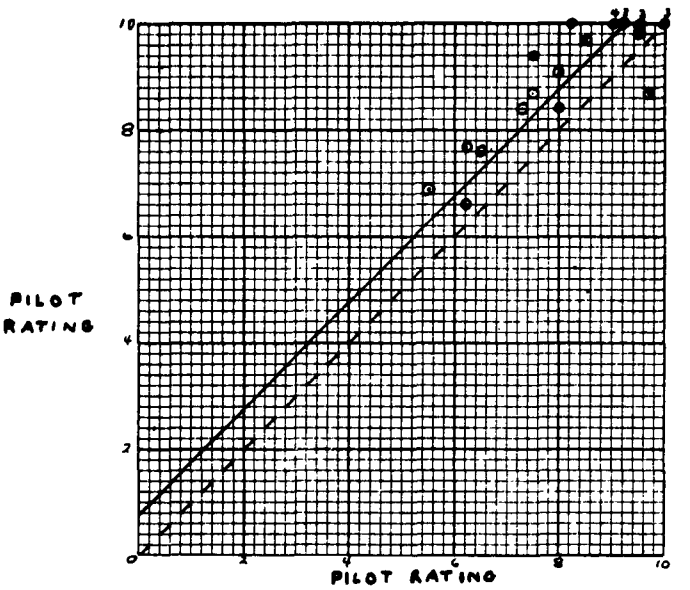

Figure 16

Method #2, Three Axis Scatter Diagram

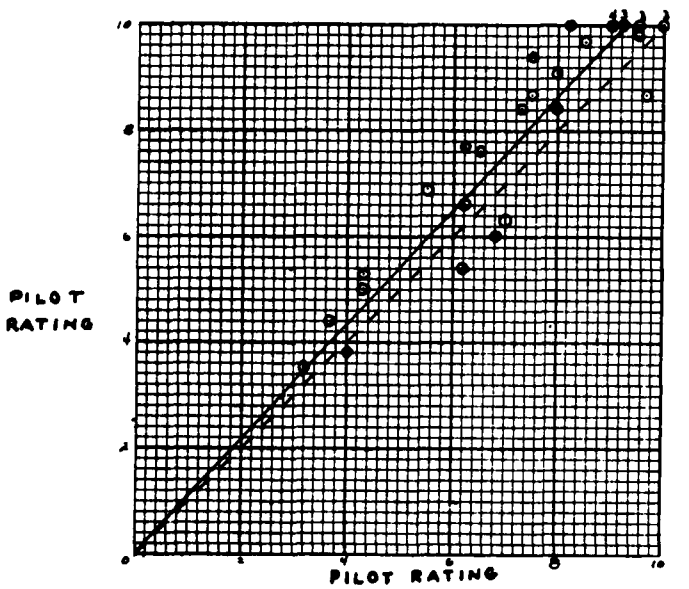

Figure 17

Method #2, Combined Data Scatter Diagram

Analysis of Method #2

Method #2 is one of the two methods that is considered promising. Although the regression line for the two axis experiment (Figure 15) is skewed from the correlation line, the data is well grouped around it. In the three axis cases (Figure 16) there is a definite trend to predict high by .8 of a rating point. However, if the two and three axis data is combined (Figure 17) to increase the range of points, the trend and correlation line closely approximate each other. There is a gradual tendency to predict high as the configurations become poorer. The values for (a) and (b) for method #2 are given in Table V.

Table V
Method #2, Slope (b) and Y Intercept (a)
for Line of Regression

	a	b
Two axis data	2.00	.5997
Three axis data	.77	1.0011
Combined data	.03	1.0832

Analysis of Method #3

Method #3 is the second method that appears to be promising. The predicted ratings for the scatter diagrams were determined from the curve of Figure C-1, which is the approximate center-line of Ashkenas' band curve as taken from reference 11.

The trend of the points is reasonably close to the correlation line over the range of the data for the two and three axis experiments (Figures 18 and 19). Combining the two and three axis data to extend the range gives a line of regression that agrees almost perfectly with the correlation line (Figure 20). The values for (a) and (b) for method #3 are given in Table VI.

Table VI
Method #3, Slope (b) and Y Intercept (a) for Line of Regression

	a	b
Two axis data	1.54	.8142
Three axis data	-4.05	1.5028
Combined data	.17	1.0167

Analysis of Method #4

The scatter diagrams indicate that method #4 tends to predict higher than actual ratings. The trend is not as pronounced as in method #1, but even combining the data (Figure 23) from the two and three axis cases (Figures 21 and 22) produces a regression line that indicates a consistent prediction of one rating point high. This bias might be attributed to a poor choice of the "best" rating. However, in this study extra runs

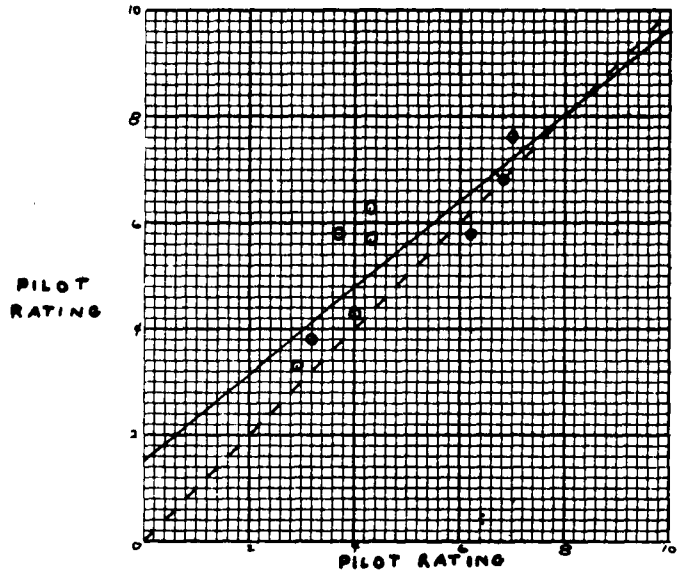

Figure 18

Method #3, Two Axis Scatter Diagram

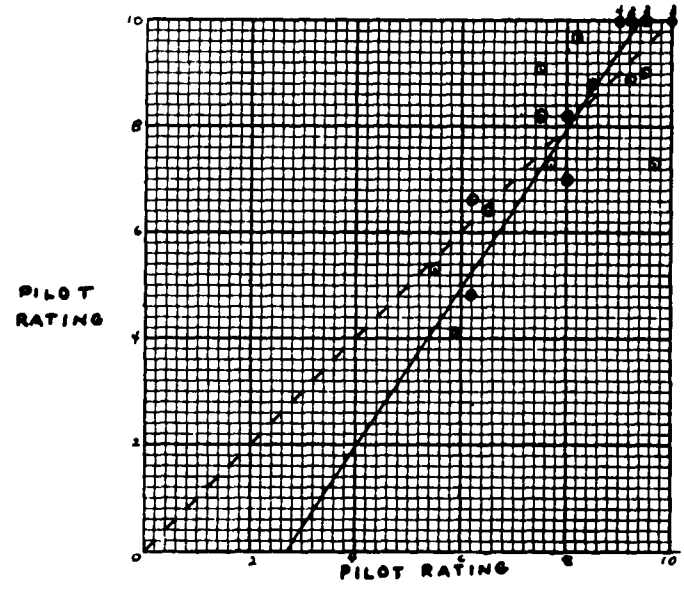

Figure 19

Method #3, Three Axis Scatter Diagram

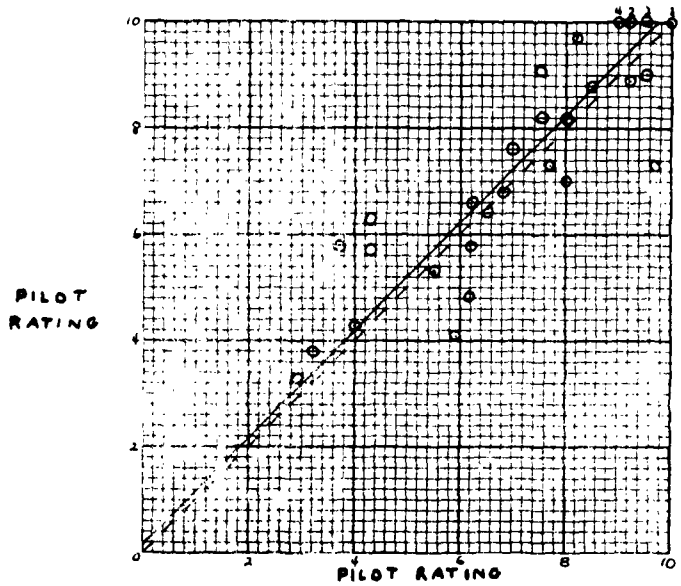

Figure 20

Method #3, Combined Data Scatter Diagram

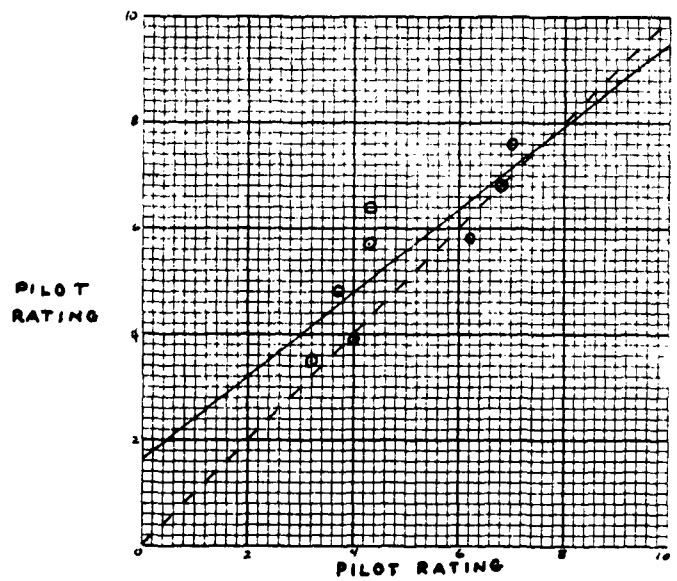

Figure 21

Method #4, Two Axis Scatter Diagram

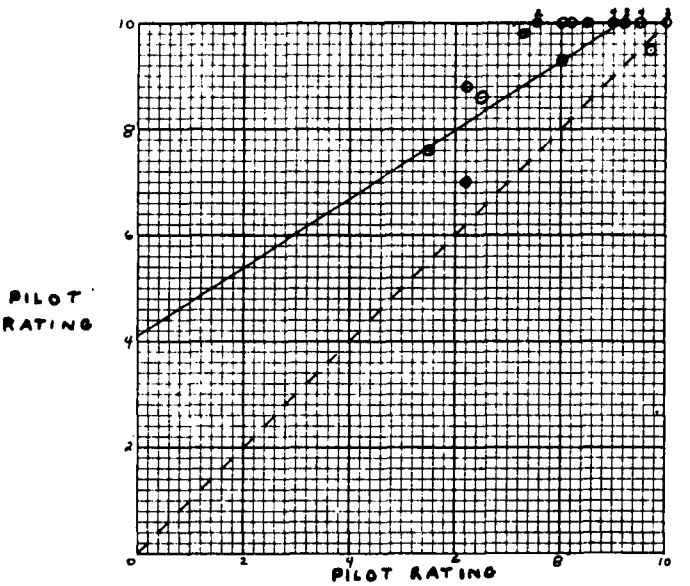

Figure 22

Method #4, Three Axis Scatter Diagram

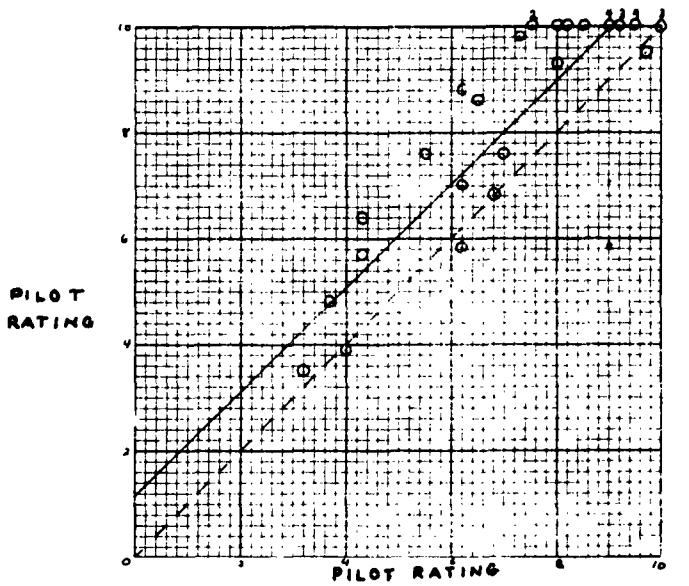

Figure 23

Method #4, Combined Data Scatter Diagram

in this configuration were flown to insure the "best" cases were well established. The values for (a) and (b) are given in Table VII.

Table VII
Method #4, Slope (b) and Y Intercept (a)
for Line of Regression

	a	b
Two axis data	1.67	.7887
Three axis data	4.14	.6456
Combined data	1.19	.9788

Comparison of Methods #2 and #3

Because of the paucity of data in the two axis experiment and the limited range of data in the three axis experiment, there is not sufficient justification at this time to make a comparison as to which method would be better for either case. However, the combined data is compared with the perfect correlation line for values of (a), (b), and sample variance in Table VIII.

The comparison shows that both methods are very good for predicting the correct rating and there is very little difference between the scatter of their points about the line of correlation.

Compared on the basis of ease and speed of calculation, method #2 is better. However, it has a major disadvantage,

since a "best" combined axis pilot rating must be determined. On the other hand, method #3 requires more time for calculations, but can be used if only single axis data is available. Because most of the experimental data in the handling qualities field has been for single axis cases, method #3 is probably the most useful.

Table VIII
Comparison of Line of Perfect Correlation with Line of Regression and Sample Variance of Method #2 and Method #3

	a	b	$\sigma^2_{Correlation}$
Line of perfect correlation	0	1.0	0
Method #2	.03	1.0832	.8838
Method #3	.17	1.0167	.8469

VI. Conclusion and Recommendations

Conclusion

This thesis has proven conclusively that a predicted pilot rating for a multiple axis system cannot be found by adding the pilot ratings of the individual axes used in the system (method #1).

It has shown that there are at least two methods for determining a predicted rating that give good results. These two methods (methods #2 and #3) were compared and it was concluded that method #3 was probably the most useful, due to the type of data that could be used with it.

It has shown that a fourth method, which utilized features of methods #2 and #3, gave poorer results than the individual methods.

Recommendations

A follow-on experiment is recommended to collect data on more test subjects. Investigation could be concentrated on the two most promising methods to determine if one gives consistently better results for a larger sample of pilots. Techniques to determine the "best" combined axis rating used in method #2 from single axis data could be investigated. Additional studies to determine if one method gives better results as the number of axes are

changed could be made. The conversion curve used in method #3 could be refined to determine if the center-line plot used in this thesis gives the best results.

Bibliography

1. Arkin, Herbert and R. R. Colton. Statistical Methods. New York: Barnes and Noble, Inc., 1956.

2. Ashkenas, I. L. and D. T. McRuer. The Determination of Lateral Handling Quality Requirements From Airframe Human-Pilot System Studies. Technical Report 59-135. Wright-Patterson Air Force Base, Ohio: Wright Air Development Center, June 1959.

3. Ashkenas, I. L., et al. Theoretical and Experimental Investigation of Some New Longitudinal Handling Qualities Parameters. Technical Report 61-26 Wright-Patterson Air Force Base, Ohio: Aeronautical Systems Division, June 1962.

4. Cooper, G. E. "Understanding and Interpreting Pilot Opinion." Aeronautical Engineering Review. 16:47-51 (March 1957).

5. Durand, T. S. and H. R. Jex. Handling Qualities in Single-Loop Roll Tracking Tasks: Theory and Simulator Experiments. Technical Document Report 62-507. Wright-Patterson Air Force Base, Ohio: Aeronautical Systems Division, May 1962.

6. Johnson, C. H. Analog Computer Techniques. New York: McGraw-Hill Book Co., Inc., 1956.

7. Kohlhaas, R. R. Limits of Controllability of a Two Axis, Unstable, Second-Order System. Unpublished thesis. Wright-Patterson Air Force Base, Ohio: Air Force Institute of Technology, March 1962.

8. McRuer, D. T., et al. Dynamics of the Airframe. Report AE-61-4II. Washington: Bureau of Aeronautics, Navy Department, September 1952.

9. McRuer, D. T., et al. A Systems Analysis View of Longitudinal Flying Qualities. Technical Report 60-43. Wright-Patterson Air Force Base, Ohio: Wright Air Development Center, January 1960.

10. Neiswanger, W. A. Elementary Statistical Methods New York: The Macmillan Co., 1956.

11. Technical Proposal No. 34. Proposal For A Theoretical Investigation of Handling Qualities for Multi-Loop, Constant Coefficient Control Situations. Unpublished Document. Wright-Patterson Air Force Base, Ohio: Wright-Patterson Air Force Base, Ohio: Wright Air Development Division, November 1960.

Appendix A

Description of Experimental Equipment

The equipment used during the experiment consisted of two analog computers, a cockpit mock-up in which a sidestick and rudder pedals were installed, an oscilloscope, a galvanic type meter (sideslip indicator), two low frequency function generators, an audio oscillator, a six channel oscillograph, and simple passive circuit elements. A general view of the experimental set-up is shown in Figure A-1.

Analog Computer

The control and reference voltage circuits of the two Goodyear Model L-3 analog computers were connected to operate both units from a single control. Input generators #3 and #4 in Figure A-2 were wired on one computer and provided sine and cosine signals with amplitudes and frequencies of 1.15 volts at .816 radians/second and 1.64 volts at 1.32 radians/second.

The controlled elements $\frac{\Theta}{\delta a_s}$, $\frac{\Phi}{\delta a_s}$, $\frac{\theta}{\delta r_p}$, and the summing points were mechanized using the rest of the computer elements. Schematic diagrams of $\frac{\Theta}{\delta a_s}$, $\frac{\Phi}{\delta a_s}$, and $\frac{\theta}{\delta r_p}$ are shown in Figures A-3, A-4, and A-5. The values for $\frac{1}{T_{p_\theta}}$, $\int_\phi$, and $\int_\theta$ were varied with pots A, B, C, and D of the schematics. Figure A-2 shows the summing points

used to generate the random input signals. Input generators #1 and #2 were Hewlett-Packard function generators producing sine waves of 4.8 volts at .367 radians/second and 5.5 volts at .483 radians/second. The inputs were compared with the outputs of the controlled elements (Θ , Φ , Ψ) and the results (Θ_ϵ , Φ_ϵ , Ψ_ϵ) were fed to the displays.

Because of the sensitivity of the sideslip needle, the Ψ voltage was reduced by a 40 kilohm resistor which brought the needle deflections within the desired range. The pitch error voltage was reduced through a sign changer and summed with the output of the bank error circuit. The operation of the bank circuit is discussed in detail in the next section.

Pitch and Bank Display Circuit

A realistic pitch and bank display was generated by the circuit shown in Figure A-6.

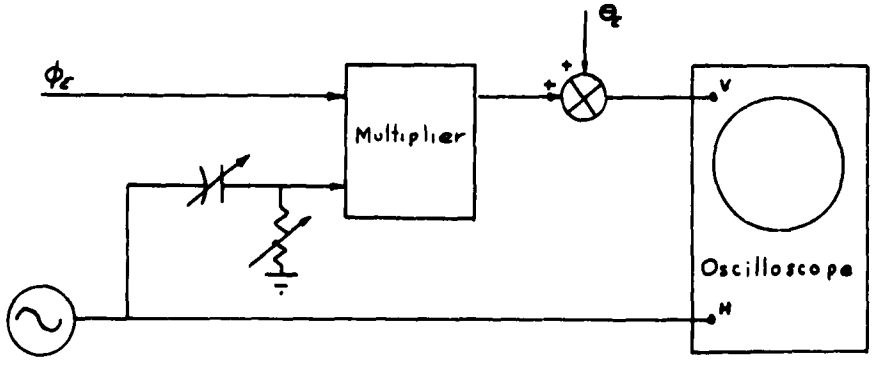

Figure A-6

Circuit for Pitch and Bank Display

A 50 cycle sine wave was fed to the horizontal sweep of the oscilloscope and to an electronic multiplier where it was multiplied by the bank error signal, Φ_ϵ . The results of the multiplication was then summed with the pitch error signal, Θ_ϵ , and fed to the vertical input of the scope. Because of the phase relationships of the horizontal and vertical inputs, the bank angle of the bar was a direct function of the bank error signal. The vertical movement of the center of the bar was a direct function of the pitch error signal. The RC circuit was placed in the input lead of the 50 cycle signal to the electronic multiplier to compensate for the phase shift introduced by the multiplier.

Cockpit Mock-up

The location of the displays and control devices in the cockpit are shown in Figures A-7 and A-8. A detailed sketch of the sidestick is illustrated in Figure A-9.

Control Devices

The pilot controlled pitch and bank with a side-stick mounted as illustrated in Figure A-7. The sidestick, an B-6 Autopilot Control Stick, manufactured by Minneapolis-Honeywell, had been modified by removing rate damping devices, leaving only spring restrainers. The maximum

deflection of $\pm 20^{\circ}$ in each axis required approximately $2\frac{1}{2}$ pounds pressure at the handgrip. Because of the greater distance to the axis of lateral movement than to the axis of longitudinal movement the pilot was required to move the stick a greater linear distance laterally than longitudinally for the same amount of angular deflection. The stick had a mechanical deadband of approximately $\pm 1^{\circ}$ longitudinally and $\pm \frac{1}{2}^{\circ}$ laterally.

The rudder pedals, used to control the sideslip needle, were spring restrained as shown in Figure A-10. A deflection of approximately $\pm$ 2 inches required about 40 pounds of pressure. The rudder force versus rudder deflection characteristics are shown in Figure A-11.

The wiring for the control devices is shown in Figure A-12. Each axis of the sidestick was mechanically linked to the arm of a 400 ohm potentiometer. The rudder pedals were connected mechanically through a pulley arrangement to the arm of a 50 kilohm rotary potentiometer. The electrical outputs of the potentiometer arms were fed to amplifiers 1, 2, and 3 (Figures A-3, A-4, and A-5). Three trim potentiometers, tied in parallel with the control potentiometers, were also fed to these amplifiers to provide a means of bringing the electrical input to zero when the control was not

deflected. Power to the potentiometers was supplied by the computer reference voltages (±200 VDC). However, because of the low power ratings of the 400 ohm pots, it was necessary to reduce this to ±5 volts with large variable resistors in series. The computer ground was used as center tap for the pots with the opposite polarities applied to each end. Two Zener diodes kept the voltage regulated very close to 5 volts. The voltage output versus physical deflection characteristics of the control devices illustrated in Figures A-13, A-14, and A-15, were measured at the output leads of Figure A-12 with a constant ±5 VDC across the pots.

System Sensitivity

The display sensitivities were

$$\text{Pitch} = .05 \frac{\text{inch}}{\text{volt}}$$

$$\text{Bank} = 188 \frac{\text{degrees}}{\text{volt}}$$

$$\text{Sideslip} = 5 \frac{\text{units}}{\text{volt}}$$

The control device sensitivities were

$$\text{Pitch} = .214 \frac{\text{volt}}{\text{degree}}$$

$$\text{Bank} = .25 \frac{\text{volt}}{\text{degree}}$$

$$\text{Sideslip} = .55 \frac{\text{volt}}{\text{inch}}$$

The overall sensitivities from control device to display were

$$= .0212 \ \frac{\text{inch}}{\text{degree-sec}} \quad \text{for } \frac{1}{T_{P_\theta}} = 0$$

$$\text{Pitch} = .0424 \ \frac{\text{inch}}{\text{degree}} \quad \text{for } \frac{1}{T_{P_\theta}} = -.5$$

$$= .0266 \ \frac{\text{inch}}{\text{degree}} \quad \text{for } \frac{1}{T_{P_\theta}} = -.8$$

$$\text{Bank} = .483 \ \frac{\text{degree}}{\text{degree}} \quad \text{for all } f_\phi$$

$$\text{Sideslip} = 2.03 \ \frac{\text{units}}{\text{inch}} \quad \text{for all } f_\beta$$

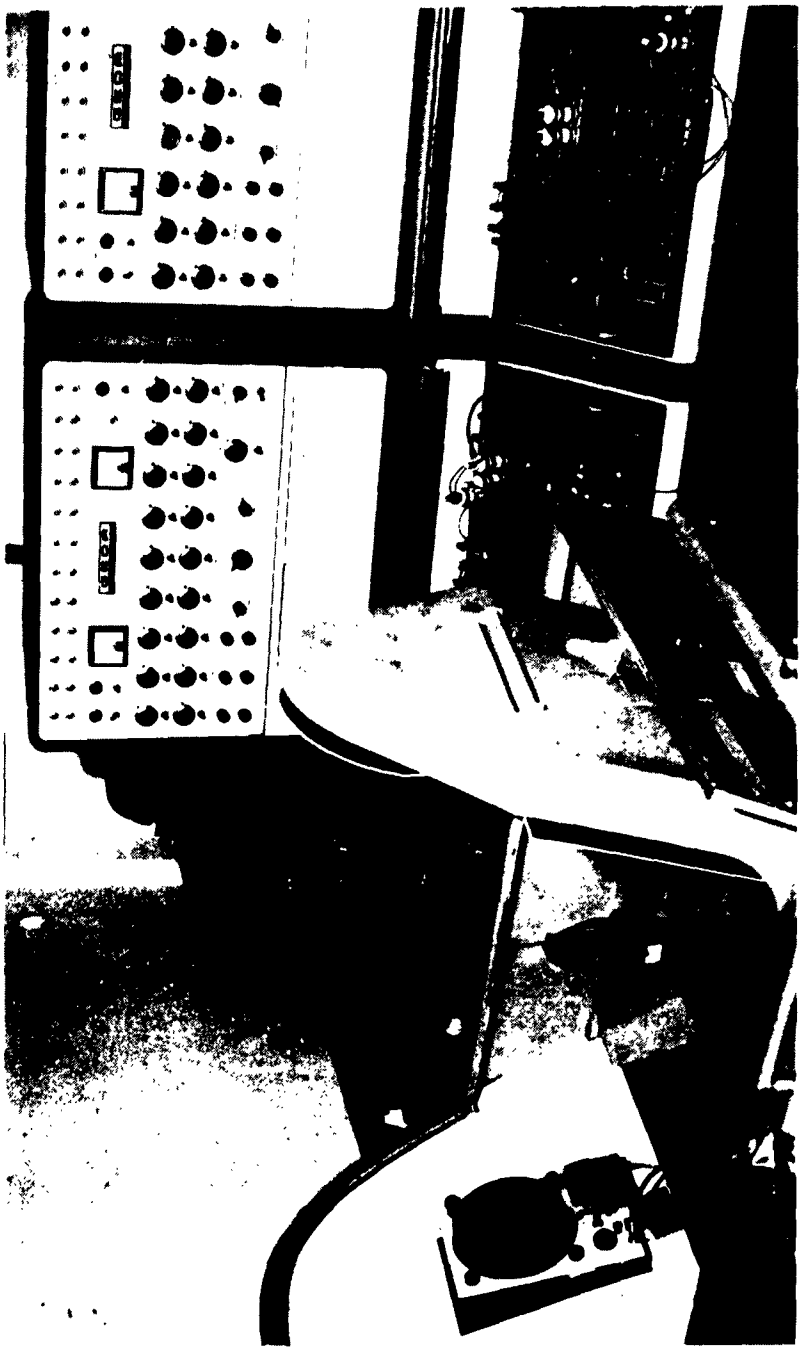

Figure A-1

General View of Simulation Equipment

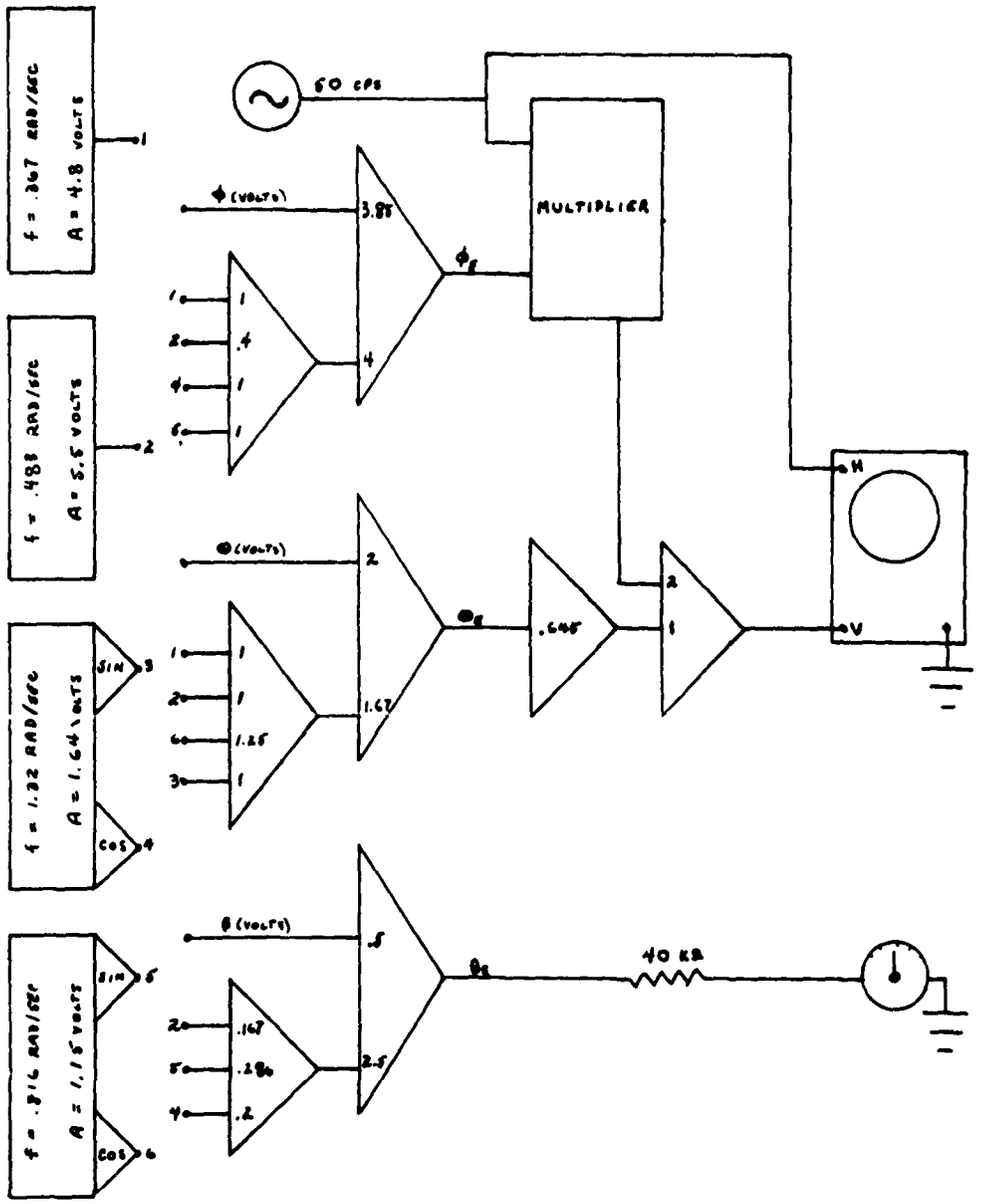

Figure A-2

Schematic Diagram of
Circuits from Summing Points to Displays

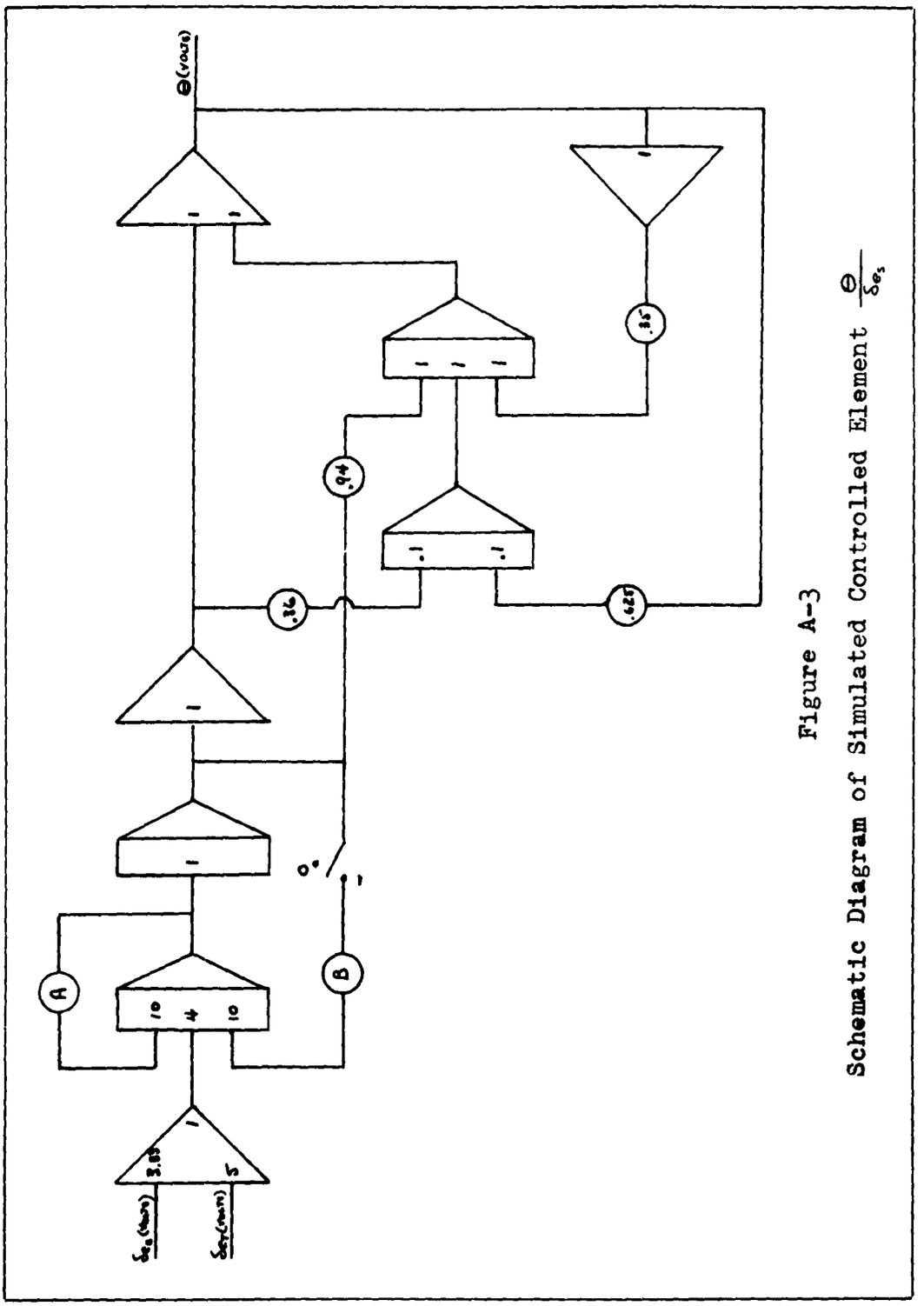

Figure A-3

Schematic Diagram of Simulated Controlled Element $\frac{\theta}{\delta e_s}$

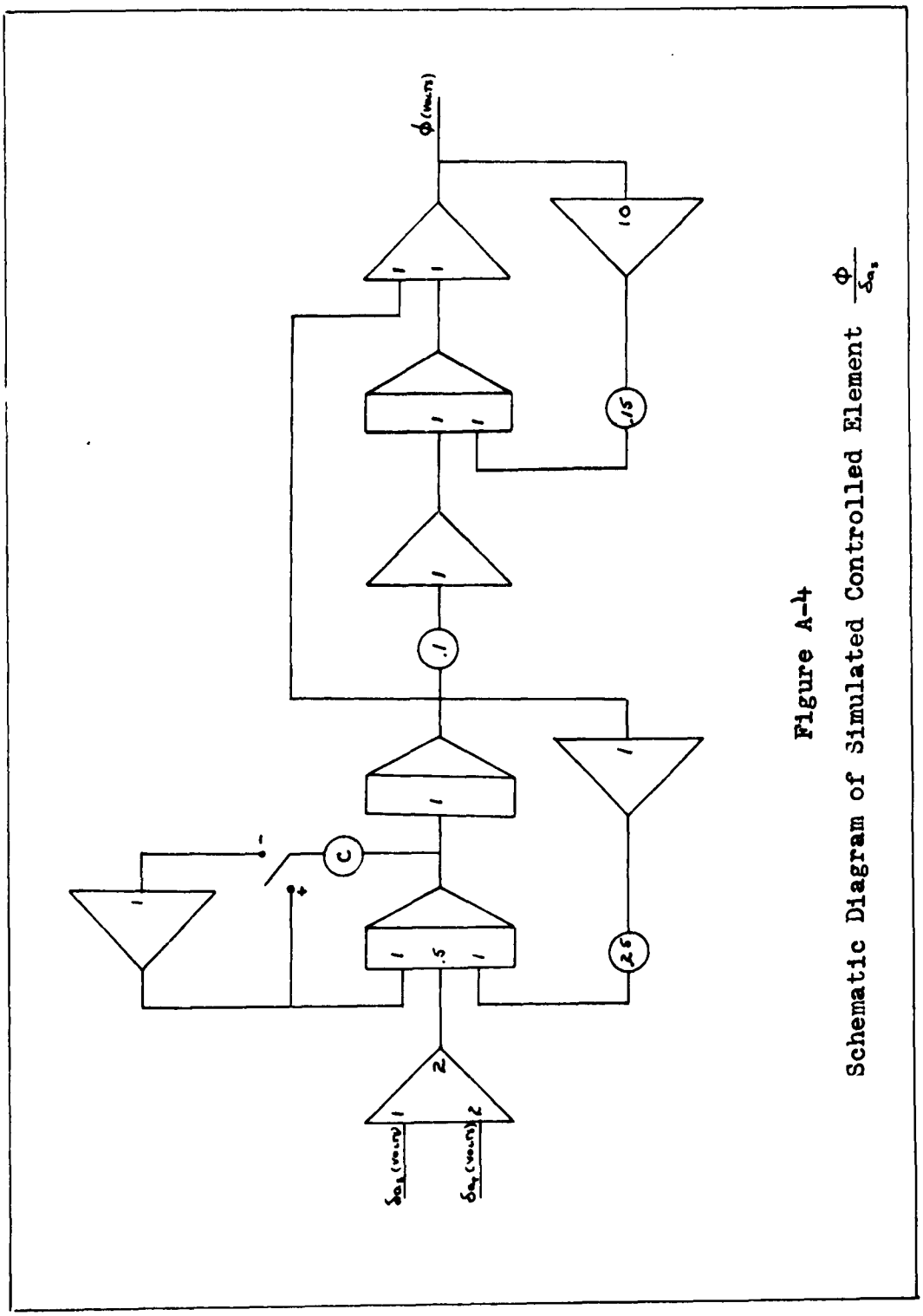

Figure A-4

Schematic Diagram of Simulated Controlled Element $\frac{\phi}{\delta_e}$

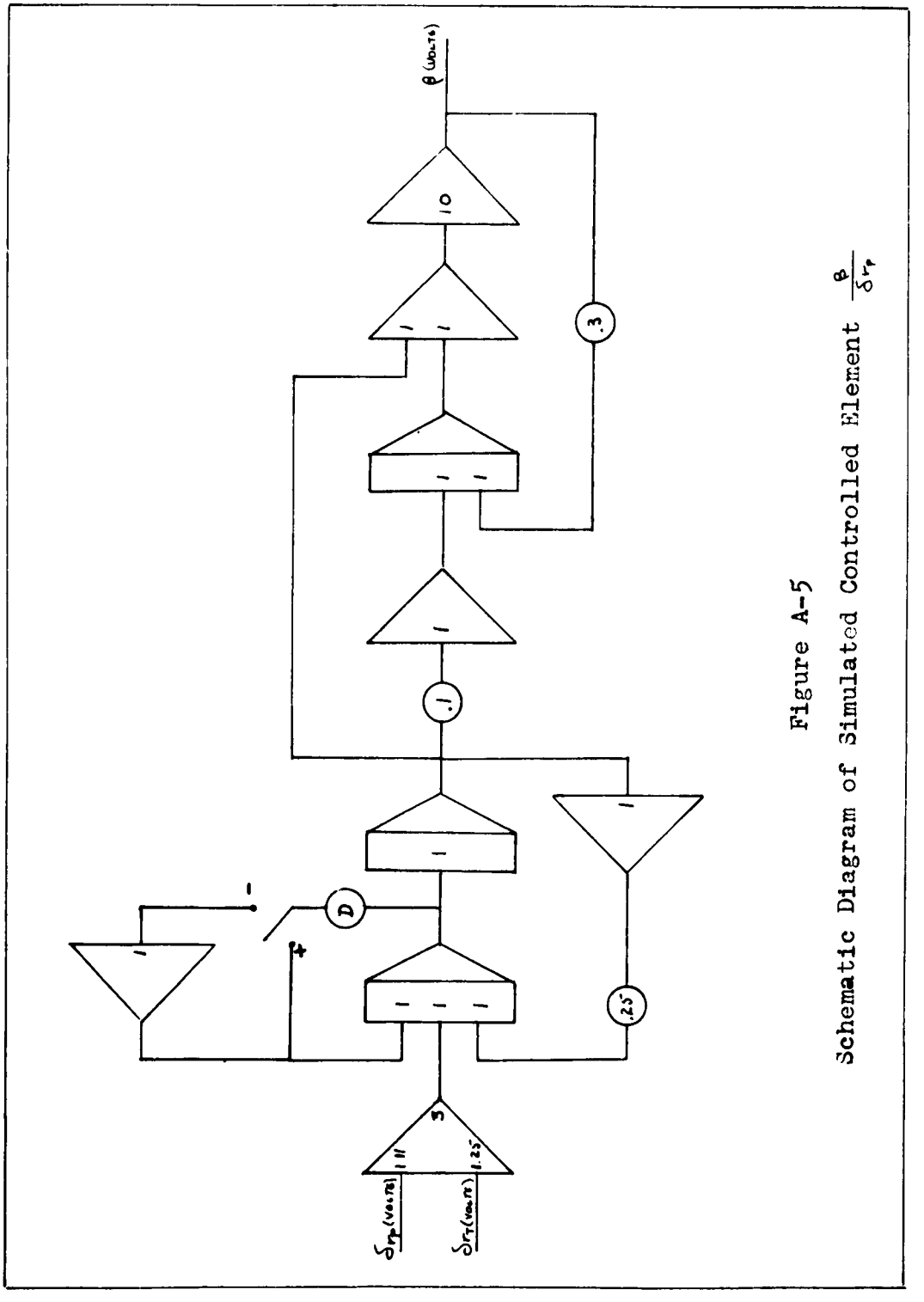

Figure A-5

Schematic Diagram of Simulated Controlled Element $\frac{\theta}{\delta r_p}$

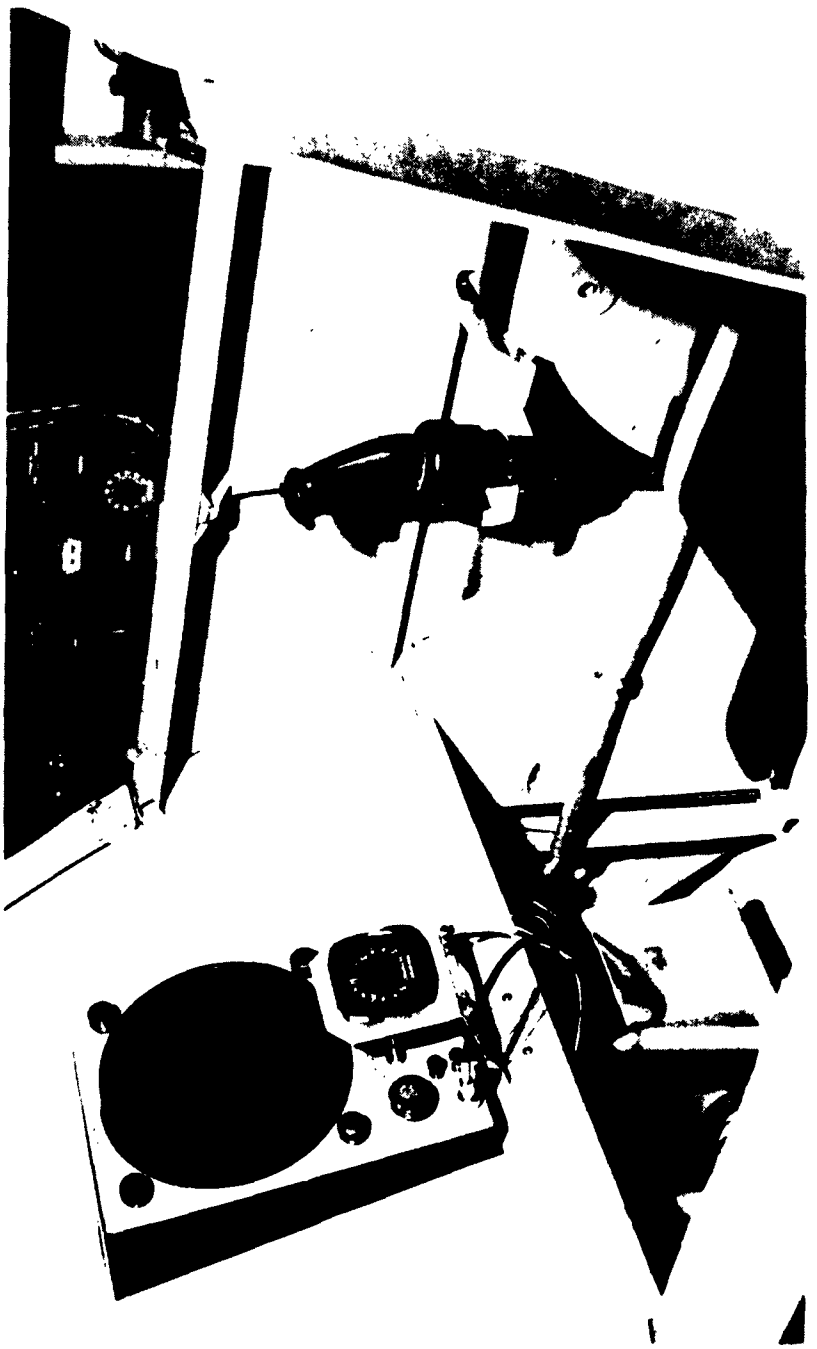

Figure A-7
Close-up View of Cockpit

(Adapted from Ref 7)

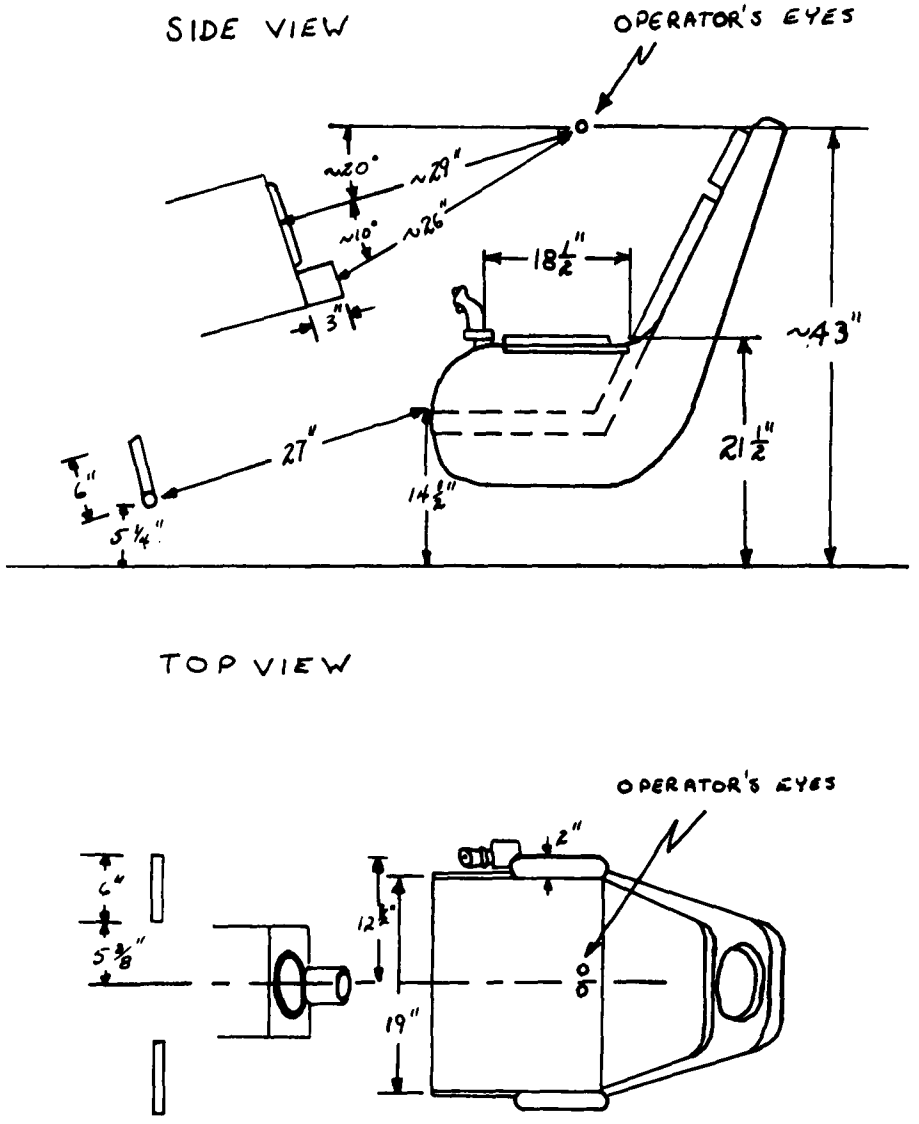

Figure A-8

Sketch of Cockpit Equipment Layout

(Adapted from Ref 7)

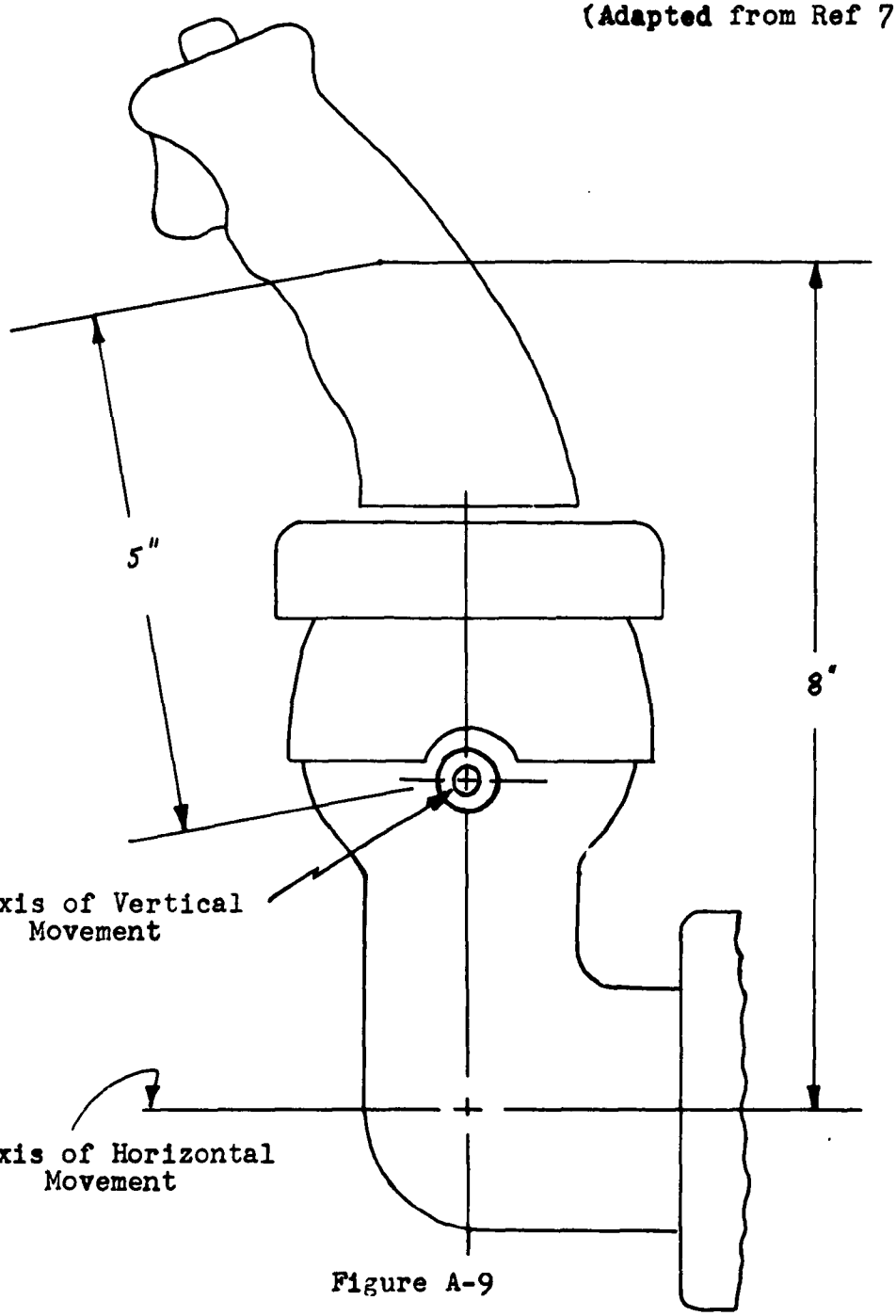

Figure A-9

Sketch of Control Stick

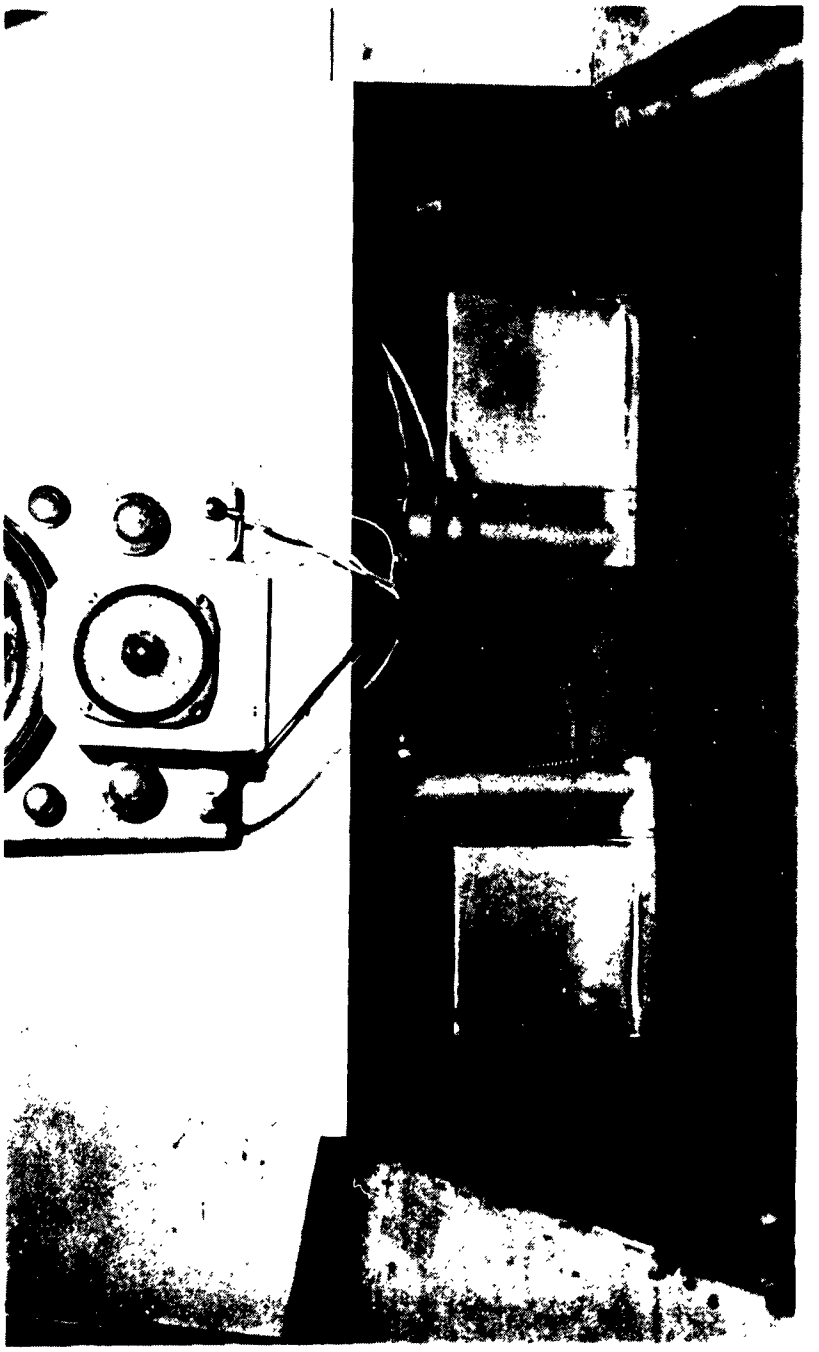

Figure A-10
Close-up View of Rudder Pedals

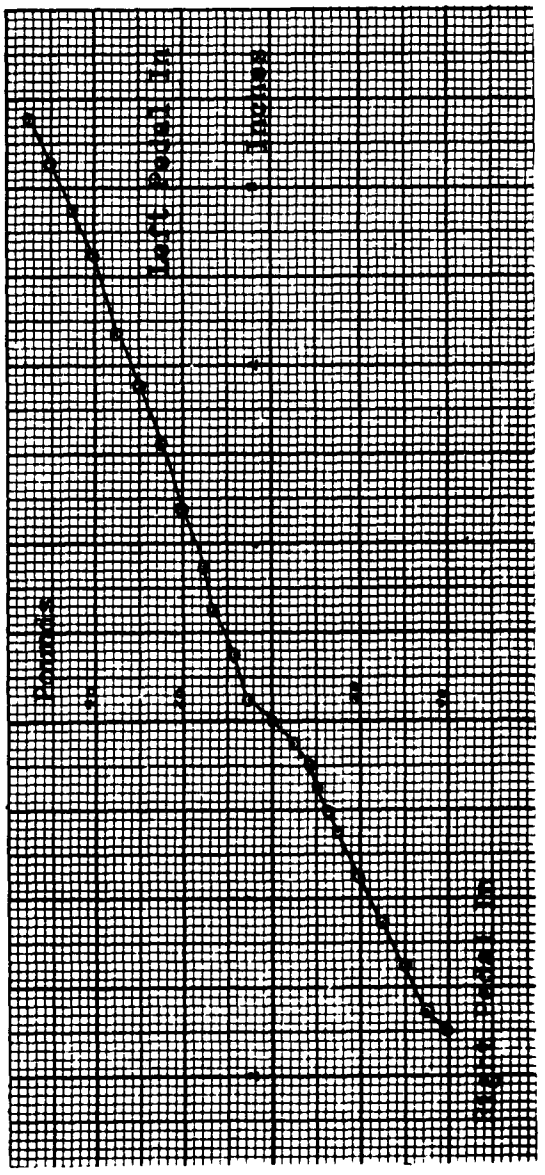

Figure A-11

Rudder Deflection versus Applied Pressure

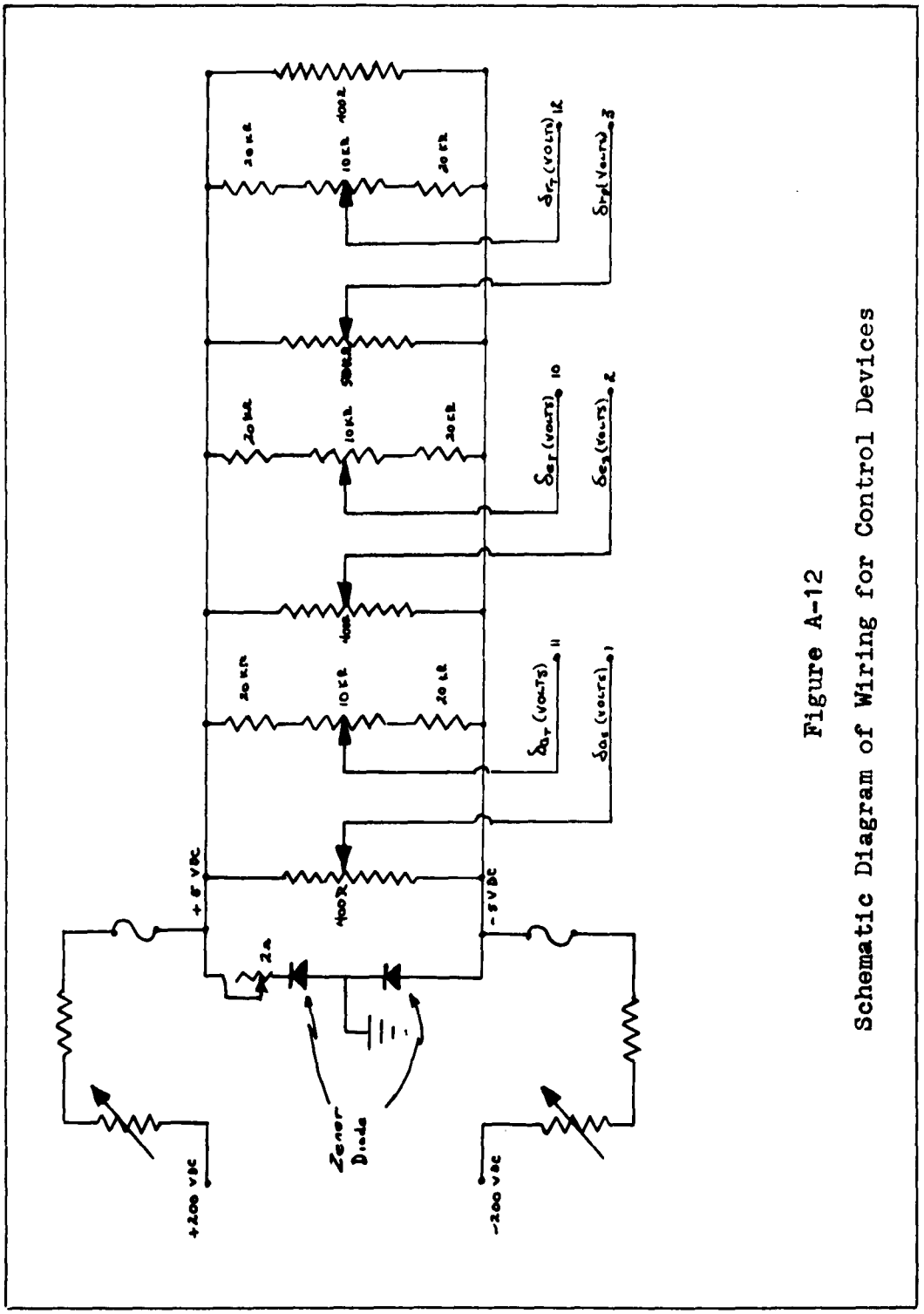

Figure A-12

Schematic Diagram of Wiring for Control Devices

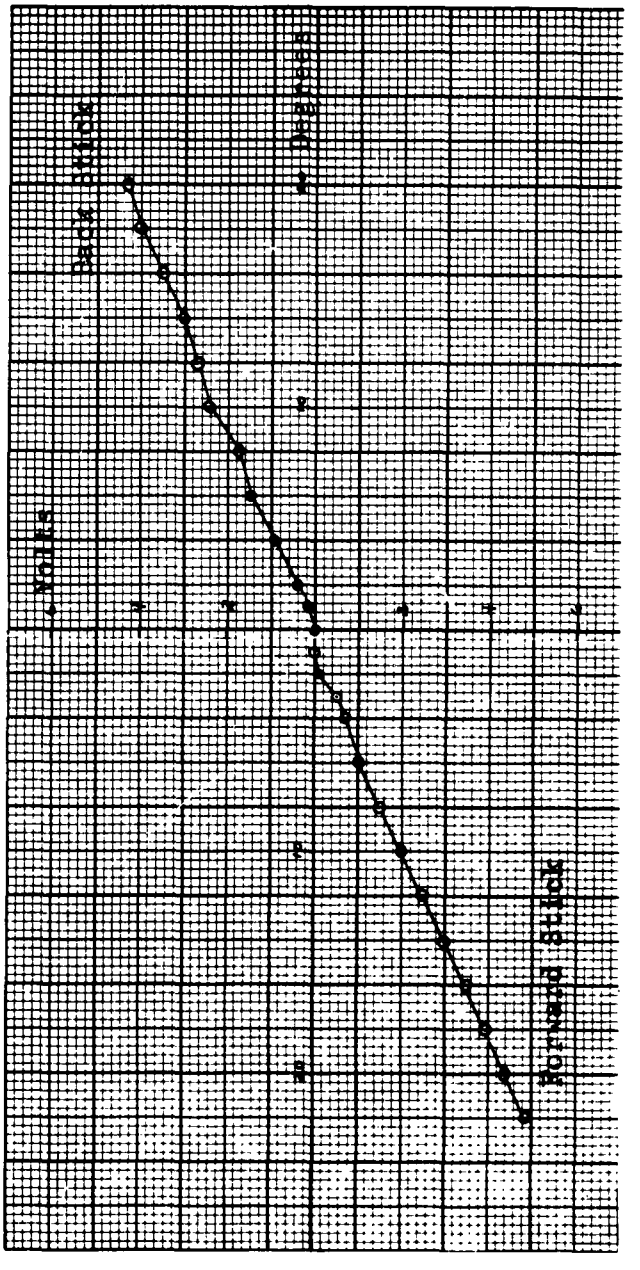

Figure A-13

Fore-Aft Sidestick Deflection versus Potentiometer Output

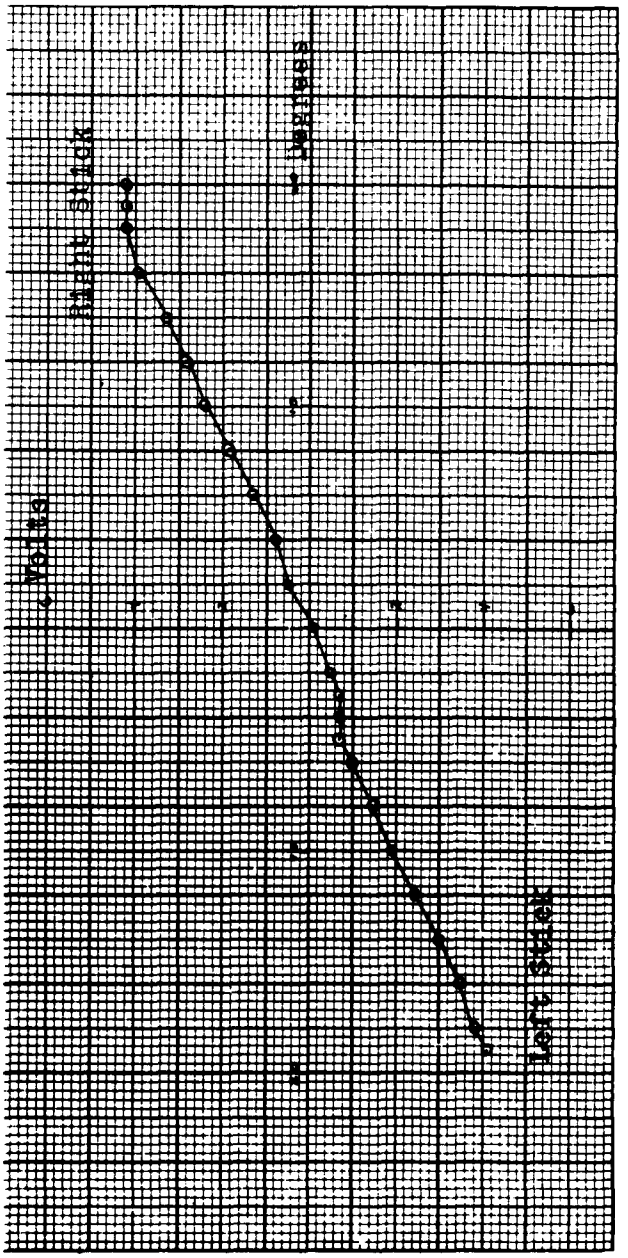

Figure A-14

Left-Right Sidestick Deflection versus Potentiometer Output

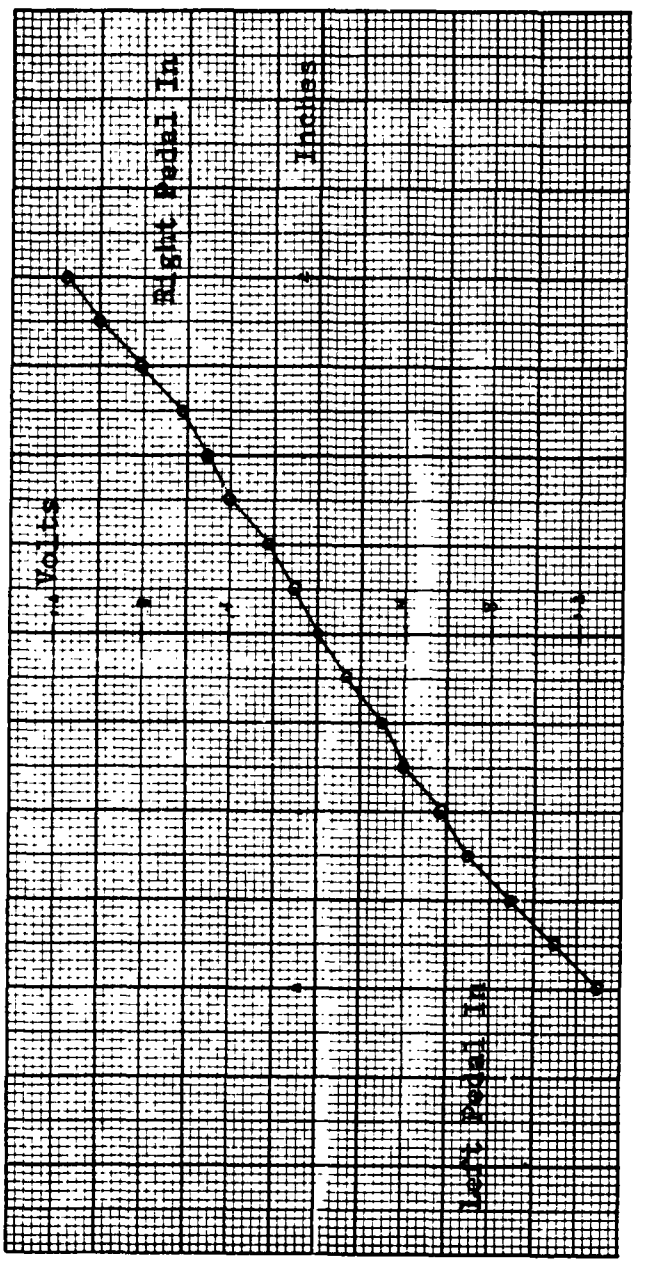

Figure A-15

Rudder Deflection versus Potentiometer Output

Appendix B

Determination of System Dynamics

Derivation of Transfer Functions

The transfer functions used in this experiment were derived from the following equations of motion for a tandem rotor helicopter:

Longitudinal

$$\dot{u} + 32.2\,\theta = -.046u + .013w - 1.48\,\dot{\theta} + .463\,\delta_{e_s}$$

$$\dot{w} - 231\,\dot{\theta} = +.046u - .900w - 1.81\,\dot{\theta} + .494\,\delta_{e_s}$$

$$\ddot{\theta} = -.00385\,u + .0148\,w - 1.85\,\dot{\theta} + .531\,\delta_{e_s}$$

Lateral - Directional

$$\dot{v} - 32.2\phi + 231\,\dot{\psi} = -152v - 2.55\,\dot{\phi} + 1.3\,\delta_{a_s} + .042\,\delta_{r_p}$$

$$\ddot{\phi} - .671\,\ddot{\psi} = -.00855\,v - 126\phi + .0187\,\dot{\psi} + .647\,\delta_{a_s} - .221\,\delta_{r_p}$$

$$\ddot{\psi} - .088\,\ddot{\phi} = +.00374v - .0084\phi - .035\,\dot{\psi} + .0057\,\delta_{a_s} + .252\,\delta_{r_p}$$

Substituting $\nu = U_{o\beta}$ and solving for the transfer functions gave the following results:

$$\frac{\Theta(S)}{\delta_{e_s}(S)} = \frac{K(S+.0426)(S+.914)}{(S-.628)(S+3.27)\left[S^2+2(.364)(.209\,S+.209^2\right]}$$

$$\frac{\phi(S)}{\delta_{a_s}(S)} = \frac{K(S-.836)(S+1)}{(S+.549)(S+1.784)(S-.016)(S-.784)}$$

$$\frac{\beta(S)}{\delta_{r_p}(S)} = \frac{K(S+.00129)(S+1.41)(S-1355)}{(S-.016)(S-.784)(S+.549)(S+1.784)}$$

To determine what effect augmentation had on the poles and zeros of the transfer functions, rate feedback in pitch and yaw were introduced into the control loop (Figure B-1).

The sensitivity, $S_A = \frac{\delta_i}{\delta_j}$, is the sensitivity of the controlled part of the airframe to the movement of the control device and is considered to be a pure gain term. Then in general

$$\delta_i = S_A\left[\delta_j - K_{\dot{A}_o} s\, A_o\right] = S_A\left[\delta_j - K_{\dot{A}_o}\dot{A}_o\right]$$

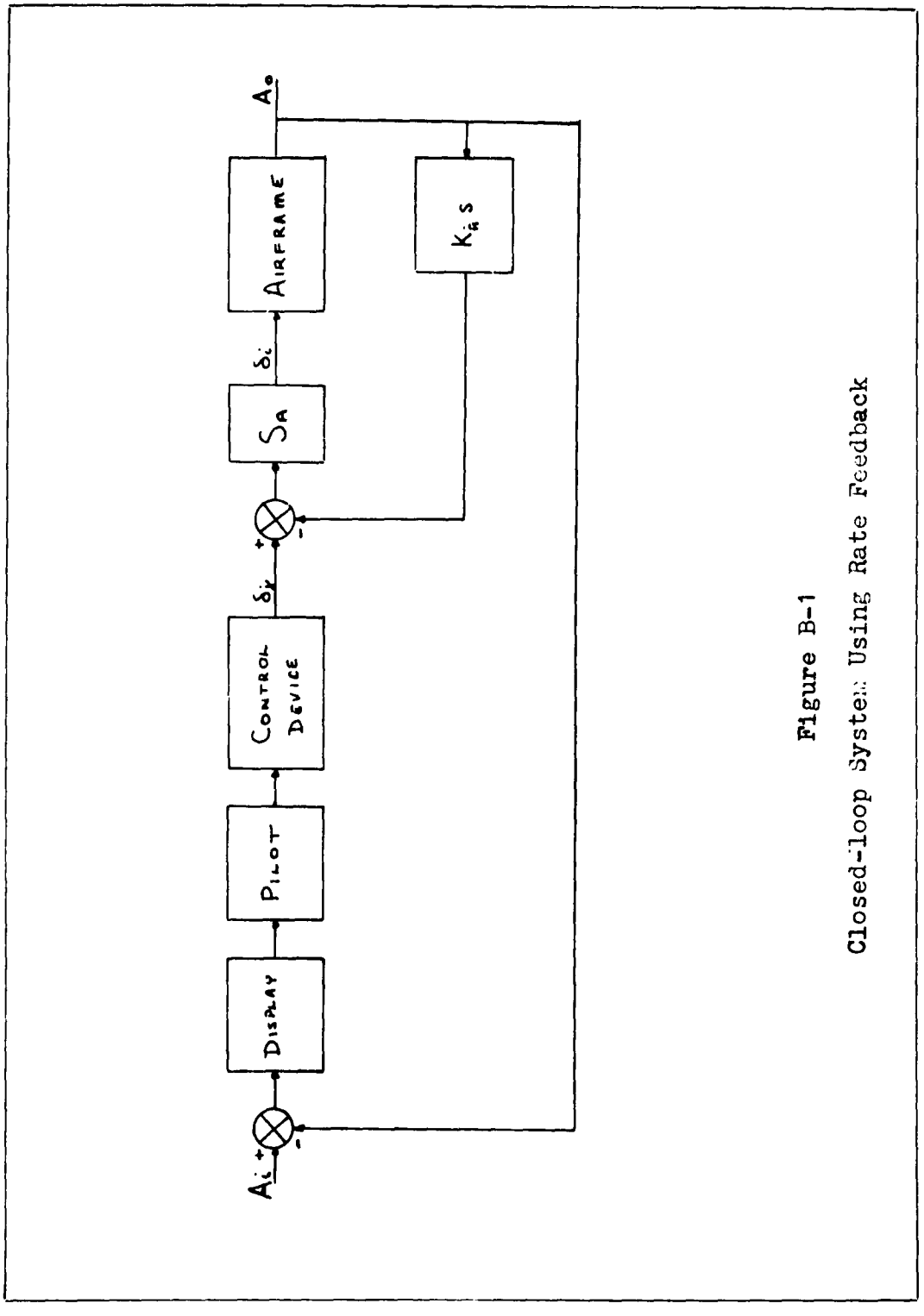

Figure B-1

Closed-loop System Using Rate Feedback

and

$$\delta_e = S_\theta \left[\delta_{e_s} - K_{\dot\theta} \dot\theta \right]$$

$$\delta_r = S_\psi \left[\delta_{r_p} - K_{\dot\psi} \dot\psi \right]$$

Substituting δ_e and δ_r into the general form of the equations of motion for this aircraft

$$\dot u + g\theta = X_u u + X_w w + X_{\dot\theta}\dot\theta + X_{\delta_e}[S_\theta(\delta_{e_s} - K_{\dot\theta}\dot\theta)]$$

$$\dot w - U_o \dot\theta = Z_u u + Z_w w + Z_{\dot\theta}\dot\theta + Z_{\delta_e}[S_\theta(\delta_{e_s} - K_{\dot\theta}\dot\theta)]$$

$$\ddot\theta = M_u u + M_w w + M_{\dot\theta}\dot\theta + M_{\delta_e}[S_\theta(\delta_{e_s} - K_{\dot\theta}\dot\theta)]$$

$$\dot v - g\phi + U_o\dot\psi = Y_v v + Y_{\dot\phi}\dot\phi + Y_{\delta_a}\delta_a + Y_{\delta_r}[S_\psi(\delta_{r_p} - K_{\dot\psi}\dot\psi)]$$

$$\ddot\phi - \frac{I_{xz}}{I_{xx}}\ddot\psi = L_v v + L_{\dot\phi}\dot\phi + L_{\dot\psi}\dot\psi + L_{\delta_a}\delta_a + L_{\delta_r}[S_\psi(\delta_{r_p} - K_{\dot\psi}\dot\psi)]$$

$$\ddot\psi - \frac{I_{xz}}{I_{zz}}\ddot\phi = N_v v + N_{\dot\phi}\dot\phi + N_{\dot\psi}\dot\psi + N_{\delta_a}\delta_a + N_{\delta_r}[S_\psi(\delta_{r_p} - K_{\dot\psi}\dot\psi)]$$

Rearranging terms

$$\dot{u} + q\theta = X_u u + X_w w + (X_{\dot{\theta}} - S_\theta X_{\delta_e} K_{\dot{\theta}})\dot{\theta} + S_\theta X_{\delta_e} \delta_{e_s}$$

$$\dot{w} - U_o \dot{\theta} = Z_u u + Z_w w + (Z_{\dot{\theta}} - S_\theta Z_{\delta_e} K_{\dot{\theta}})\dot{\theta} + S_\theta Z_{\delta_e} \delta_{e_s}$$

$$\ddot{\theta} = M_u u + M_w w + (M_{\dot{\theta}} - S_\theta M_{\delta_e} K_{\dot{\theta}})\dot{\theta} + S_\theta M_{\delta_e} \delta_{e_s}$$

$$\dot{v} - q\phi = Y_v v + Y_{\dot{\phi}} \dot{\phi} + Y_{\delta_a} \delta_a - (U_o + S_\psi Y_{\delta_r} K_{\dot{\psi}})\dot{\psi} + S_\psi Y_{\delta_r} \delta_{r_p}$$

$$\ddot{\phi} - \frac{I_{xz}}{I_{xx}} \ddot{\psi} = L_v v + L_{\dot{\phi}} \dot{\phi} + L_{\delta_a} \delta_a + (L_{\dot{\psi}} - S_\psi L_{\delta_r} K_{\dot{\psi}})\dot{\psi} + S_\psi L_{\delta_r} \delta_{r_p}$$

$$\ddot{\psi} - \frac{I_{xz}}{I_{zz}} \ddot{\phi} = N_v v + N_{\dot{\phi}} \dot{\phi} + N_{\delta_a} \delta_a + (N_{\dot{\psi}} - S_\psi N_{\delta_r} K_{\dot{\psi}})\dot{\psi} + S_\psi N_{\delta_r} \delta_{r_p}$$

Referring to the actual equations of motion

$S_\theta X_{\delta_e} = .463$ and $X_{\dot{\theta}}' = -(1.48 + .463 K_{\dot{\theta}})$

$S_\theta Z_{\delta_e} = .494$ and $Z_{\dot{\theta}}' = -(1.81 + 4.94 K_{\dot{\theta}})$

$S_\theta M_{\delta_e} = .531$ and $M_{\dot{\theta}}' = -(1.85 + .531 K_{\dot{\theta}})$

$S_\psi Y_{\delta_r} = .042$ and $U_o' = (231 + .042 K_{\dot{\psi}})$

$S_\psi L_{\delta_r} = -.221$ and $L_{\dot{\psi}}' = (.0187 + .221 K_{\dot{\psi}})$

$S_\psi N_{\delta_r} = .252$ and $N_{\dot{\psi}}' = -(.035 + .252 K_{\dot{\psi}})$

To establish an initial value for $K_{\dot{\theta}}$ the short period frequency was arbitrarily set equal to zero. Using the short period approximation (Ref 8:III-7)

$$\omega_{sp}^2 = M_{\dot{\theta}_i}' Z_w - U_o M_w = 0$$

and

$$M_{\dot{\theta}_i}' = \frac{U_o M_w}{Z_w} = -3.665$$

Substituting into the equation for $M_{\dot{\theta}_i}'$

$$K_{\dot{\theta}_i} = 3.425$$

Multiples of the initial $K_{\dot{\theta}}$ were then used to find additional values of $M_{\dot{\theta}}'$ which were substituted into the original equations of motion. The transfer functions determined are listed in Table B-I.

Analysis shows the positive pole moving toward the origin as $K_{\dot{\theta}}$ is increased. This pole was used to vary the amount of instability in pitch. Since it was not necessary to simulate a particular aircraft, the other poles and zeros were arbitrarily fixed at values approximating those for $K_{\dot{\theta}} = 3.425$. The transfer function used in pitch was

$$\frac{\theta(S)}{\delta_{e_s}(S)} = \frac{K_\phi(S+.04)(S+.9)}{(S+1/T_{P_\phi})(S+5)[S^2+2(.7)(.25)S+.25^2]}$$

Table B-I

Transfer Function $\frac{\theta(s)}{\delta_{e_s}(s)}$ for Different K_ϕ

K_ϕ	Transfer Function
0	$\frac{K(S+.0426)(S+.914)}{(S-.628)(S+3.27)[S^2+2(.364)(.209)S+.209^2]}$
3.425	$\frac{K(S+.0426)(S+.914)}{(S-.287)(S+4.58)[S^2+2(.611)(.261)S+.261^2]}$
13.7	$\frac{K(S+.0426)(S+.914)}{(S-.111)(S+9.51)(S+.504)(S+.168)}$
27.4	$\frac{K(S+.0426)(S+.914)}{(S-.0689)(S+16.6)(S+.696)(S+.113)}$

A similar approach was used in determining values for $L_{\dot{\psi}}'$ and $N_{\dot{\psi}}'$, but $K_{\dot{\psi}}$ was arbitrarily given values of 5, 10, and 20. The transfer functions determined are listed in Tables B-II and B-III.

Table B-II

Transfer Function $\frac{\phi(s)}{\delta_{a_s}(s)}$ for Different K_ψ

K_ψ	Transfer Function
0	$\frac{K(S-.836)(S+1)}{(S-.016)(S-.784)(S+.549)(S+1.784)}$
5	$\frac{K(S-.37)(S+1.8)}{(S+1.15)(S+2.18)\ [S^2-2(.546)(.462)S+.462^2]}$
10	$\frac{K(S-.179)(S+2.87)}{(S+1.38)(S+2.79)\ [S^2-(.340)(.495)S+.495^2]}$
20	$\frac{K(S-.0359)(S+5.25)}{(S+1.51)(S+5.18)\ [S^2-2(.205)(.513)S\ +.513^2]}$

As K_ψ increases the set of complex positive poles moves to the left. The stability of this axis was varied by changing the damping ratio of these poles. A further simplification was made by cancelling the pole and zero that are approximately equal for K_ψ =10 and 20. The positive zero was moved to the left-hand side of the s-plane to improve the overall closed loop stability. The final form of the bank equation was

$$\frac{\Phi(S)}{\delta_{a_s}(S)} = \frac{K_\phi(S+.1)}{(S+1.5)\left[S^2+2\zeta_\phi(5)S+.5^2\right]}$$

Table B-III

Transfer Function $\frac{\beta(s)}{\delta r_p(s)}$ for Different K_ψ

K_ψ	Transfer Function
0	$\frac{K(S+.00129)(S+1.41)(S-1355)}{(S-.016)(S-.784)(S+.549)(S+1.784)}$
5	$\frac{K(S+.00129)(S+1.41)(S-1355)}{(S+1.15)(S+2.12)\ [S^2-2(.546)(.462)S+.462^2]}$
10	$\frac{K(S+.0220)(S+1.30)(S-1353)}{(S+1.30)(S+2.97)\ [S^2-2(.340)(.495)S+.495^2]}$
20	$\frac{K(S+.001)(S+1.41)(S-1351)}{(S+1.51)(S+5.18)\ [S^2-2(.205)(.513)S+.513^2]}$

The same procedure was used in determing that the damping ratio would be used in adjusting the stability in sideslip and the pole-zero set was again cancelled. The large positive zero has the effect of making the function negative. The function

$$\frac{\beta(S)}{\delta r_p(S)} = \frac{K_\beta S}{(S+3)[S^2+2\zeta_\beta(.5)S+.5^2]}$$

was adopted for the initial trials in the simulator. However, the operator was not able to control the sideslip indicator within desirable display limits. Therefore, the function

$$\frac{\beta(S)}{\delta r_p(S)} = \frac{K_\beta(S+.1)}{(S+3)[S^2+2\zeta_\beta(.5)S+.5^2]}$$

was used.

Determination of Augmentation Levels

The particular settings on the computer for each augmentation level were selected by first estimating values of $\frac{1}{T_{p_\theta}}$, f_ϕ, and f_β that would produce a rating in each major category of the Cooper scale. A pilot (the author) who was not flying the data runs then flew and rated single axis runs for these settings. Adjustments were made in the settings until he was rating the "H" level at 2, and "M" level at 4, and the "L" level at 6. The values at these settings were then fixed for the rest of the experiment.

Appendix C

Data and Curve Used in Calculations

Conversion Curve

The curve used to determine the predicted pilot ratings in method #3 and #4 is shown in Figure C-1. It is the approximate center line of the band curve proposed by Ashkenas in reference 11.

Raw Data

The raw data taken during the experiment is listed in Table C-I. It is available for checking the calculated results shown in this thesis. It can also be used for other problems.

Numbers Used In Calculations

The numbers used in all calculations were averaged values of the ratings for any particular configuration. These numbers are given in Tables C-II, C-III, C-IV, and C-V.

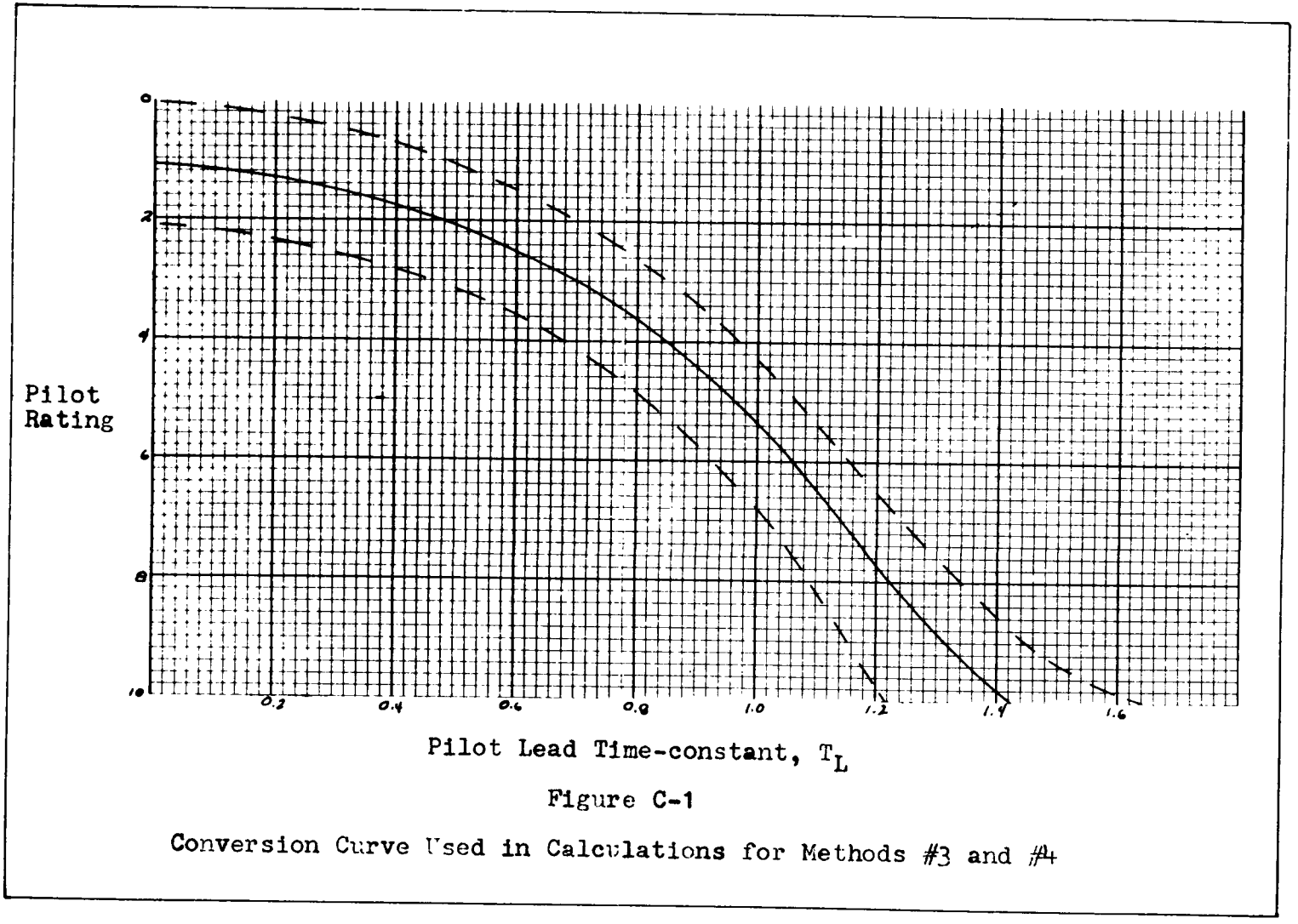

Figure C-1

Conversion Curve Used in Calculations for Methods #3 and #4

Table C-I
Raw Data for All Data Runs

Three Axis Experiment

Data Run #1
Single Axis - 120 seconds

Run	Configuration θ	Configuration φ	Configuration β	Pilot Rating	Run	Configuration θ	Configuration φ	Configuration β	Pilot Rating
1	M			4.0	12		H		3.0
2	L			6.5	13	L			7.0
3		H		2.5	14	H			2.5
4		L		6.0	15	M			4.5
5			M	4.0	16		M		3.5
6			H	3.5	17		L		5.5
7	L			8.0	18		H		3.0
8	H			2.5	19			H	3.5
9			M	4.5	20			L	7.0
10			L	7.0	21			M	3.0
11		M		4.0					

Data Run #2
Three Axis - 120 seconds

Run	Configuration θ	Configuration φ	Configuration β	Pilot Rating	Run	Configuration θ	Configuration φ	Configuration β	Pilot Rating
22	H	L	H	-*	24	M	M	M	-
23	H	L	H	9.0	25	M	M	M	8.0

* Pilot exercised re-run option

Run	Configuration θ	ϕ	β	Pilot Rating	Run	Configuration θ	ϕ	β	Pilot Rating
26	L	M	M	-	49	L	H	M	10.0
27	L	M	M	9.0	50	M	H	H	6.5
28	H	H	L	-	51	H	H	M	6.5
29	H	H	L	10.0	52	L	L	L	-
30	L	L	M	-	53	L	L	L	-
31	L	L	M	10.0	54	L	L	L	10.0
32	H	L	M	-	55	H	M	H	6.0
33	H	L	M	8.0	56	L	L	H	-
34	M	L	L	-	57	L	L	H	9.5
35	M	L	L	10.0	58	L	H	H	-
36	H	M	L	-	59	L	H	H	10.0
37	H	M	L	9.0	60	H	L	L	-
38	H	H	H	6.0	61	H	L	L	9.5
39	L	M	H	-	62	M	L	M	-
40	L	M	H	9.0	63	M	L	M	9.5
41	M	H	M	8.0	64	L	H	L	-
42	M	M	H	7.5	65	L	H	L	10.0
43	L	M	L	-	66	M	M	L	-
44	L	M	L	9.5	67	M	M	L	9.0
45	M	H	L	-	68	H	M	M	7.0
46	M	H	L	9.5	69	M	L	H	-
47	L	H	M	-	70	M	L	H	8.5
48	L	H	M	-	71	H	H	H	5.5

Data Run #3
Three Axis Repeated Runs - 120 seconds

Run	Configuration θ	ϕ	β	Pilot Rating	Run	Configuration θ	ϕ	β	Pilot Rating
72	H	L	H	-	90	H	H	L	9.0
73	H	L	H	7.0	91	L	L	H	-
74	L	H	H	-	92	L	L	H	8.5
75	L	H	H	9.0	93	M	L	H	8.0
76	L	M	L	-	94	H	M	M	6.0
77	L	M	L	9.0	95	H	H	L	-
78	M	H	H	6.5	96	H	H	L	10.0
79	L	L	M	-	97	M	H	L	-
80	L	L	M	-	98	M	H	L	-
81	L	L	M	9.0	99	M	H	L	9.0
82	M	H	M	7.5	100	H	M	L	-
83	H	H	H	6.0	101	H	M	L	-
84	M	M	M	7.0	102	H	M	L	8.0
85	H	H	M	6.0	103	H	M	H	5.0
86	L	H	M	-	104	M	H	M	6.5
87	L	H	M	8.5	105	M	H	H	5.5
88	H	H	L	-	106	H	M	H	5.5
89	H	H	L	-	107	H	H	H	6.0

Data Run #4
Single Axis Repeated Runs - 60 seconds

Run	Configuration θ	Configuration φ	Configuration ℯ	Pilot Rating	Run	Configuration θ	Configuration φ	Configuration ℯ	Pilot Rating
108		M		4.0	120	L			6.0
109		L		5.0	121	H			3.0
110			M	4.5	122	M			5.0
111			H	3.5	123	H			3.0
112	M			4.5	124		H		4.0
113	L			6.0	125		M		4.5
114			L	6.0	126		M		5.0
115			M	4.5	127		L		6.5
116		M		5.0	128			L	5.0
117		H		4.0	129			H	3.5
118	H			3.0	130			H	3.0
119	M			5.0	131			M	4.0

Two Axis Experiment

Data Run #5
Single Axis - 60 seconds

Run	Configuration θ	Configuration φ	Pilot Rating	Run	Configuration θ	Configuration φ	Pilot Rating
132	H		3.0	136	H		3.0
133	M		3.5	137	M		3.5
134	L		4.0	138	H		3.0
135	L		3.5	139	H		2.5

Run	Configuration θ	Configuration φ	Pilot Rating	Run	Configuration θ	Configuration φ	Pilot Rating
140	L		4.0	145		H	3.0
141		H	3.0	146		H	4.0
142		M	4.5	147		L	6.0
143		M	5.0	148		L	5.5
144		L	6.5	149		L	5.0

Data Run #6
2 Axis - 120 seconds

Run	Configuration θ	Configuration φ	Pilot Rating	Run	Configuration θ	Configuration φ	Pilot Rating
150	M	M	4.0	165	L	L	7.0
151	H	M	3.0	166	H	M	4.0
152	H	H	2.0	167	H	H	3.0
153	M	H	3.5	168	M	M	4.0
154	L	H	4.0	169	M	M	5.0
155	M	L	6.5	170	L	L	7.0
156	L	M	4.0	171	M	H	3.0
157	L	L	7.0	172	H	H	3.5
158	H	L	6.0	173	L	M	4.0
159	H	M	4.0	174	L	M	5.0
160	H	H	3.0	175	H	L	6.5
161	M	H	3.0	176	L	H	4.0
162	L	H	4.0	177	M	L	7.0
163	H	H	3.0	178	H	L	6.0
164	M	L	7.0				

Table C-II
Averaged Values of Single Axis Runs
for Two Axis Experiment

Pitch	Bank
H - 2.9	H - 3.3
M - 3.5	M - 4.8
L - 3.8	L - 5.8

Table C-III
Averaged Values for Two Axis Runs

Configuration		Pilot Rating	Configuration		Pilot Rating
θ	ϕ		θ	ϕ	
H	H	2.9	M	L	6.8
H	M	3.7	L	H	4.0
H	L	6.2	L	M	4.3
M	H	3.2	L	L	7.0
M	M	4.3			

Table C-IV
Averaged Values of Single Axis Runs
for Three Axis Experiment

Pitch	Bank	Sideslip
H - 2.8	H - 3.3	H - 3.4
M - 4.6	M - 4.3	M - 4.1
L - 6.7	L - 5.8	L - 6.2

Table C-V
Averaged Values of Three Axis Runs

Configuration			Pilot Rating	Configuration			Pilot Rating
θ	ϕ	β		θ	ϕ	β	
H	H	H	5.9	M	M	L	9.0
H	H	M	6.2	M	L	H	8.2
H	H	L	9.7	M	L	M	9.5
H	M	H	5.5	M	L	L	10.0
H	M	M	6.5	L	H	H	9.5
H	M	L	8.5	L	H	M	9.2
H	L	H	8.0	L	H	L	10.0
H	L	M	8.0	L	M	H	9.0
H	L	L	9.5	L	M	M	9.0
M	H	H	6.2	L	M	L	9.2
M	H	M	7.3	L	L	H	9.0
M	H	L	9.2	L	L	M	9.5
M	M	H	7.5	L	L	L	10.0
M	M	M	7.5				